

# An Unstaggered Constrained Transport Method for the 3D Ideal Magnetohydrodynamic Equations

Christiane Helzel<sup>a</sup>, James A. Rossmanith<sup>b,1</sup>, Bertram Taetz<sup>a</sup>

<sup>a</sup>*Fakultät für Mathematik, Ruhr-Universität Bochum, 44780 Bochum, Germany*

<sup>b</sup>*Department of Mathematics, University of Wisconsin, 480 Lincoln Drive, Madison, WI 53706-1388, USA*

---

## Abstract

Numerical methods for solving the ideal magnetohydrodynamic (MHD) equations in more than one space dimension must either confront the challenge of controlling errors in the discrete divergence of the magnetic field, or else be faced with nonlinear numerical instabilities. One approach for controlling the discrete divergence is through a so-called *constrained transport* method, which is based on first predicting a magnetic field through a standard finite volume solver, and then correcting this field through the appropriate use of a magnetic vector potential. In this work we develop a constrained transport method for the 3D ideal MHD equations that is based on a high-resolution wave propagation scheme. Our proposed scheme is the 3D extension of the 2D scheme developed by Rossmanith [*SIAM J. Sci. Comp.* **28**, 1766 (2006)], and is based on the high-resolution wave propagation method of Langseth and LeVeque [*J. Comp. Phys.* **165**, 126 (2000)]. In particular, in our extension we take great care to maintain the three most important properties of the 2D scheme: (1) all quantities, including all components of the magnetic field and magnetic potential, are treated as cell-centered; (2) we develop a high-resolution wave propagation scheme for evolving the magnetic potential; and (3) we develop a wave limiting approach that is applied during the vector potential evolution, which controls unphysical oscillations in the magnetic field. One of the key numerical difficulties that is novel to 3D is that the transport equation that must be solved for the magnetic vector potential is only weakly hyperbolic. In presenting our numerical algorithm we describe how to numerically handle this problem of weak hyperbolicity, as well as how to choose an appropriate gauge condition. The resulting scheme is applied to several numerical test cases.

*Keywords:* magnetohydrodynamics, constrained transport, hyperbolic conservation laws, plasma physics, wave propagation algorithms

---

*Email addresses:* `Christiane.Helzel@ruhr-uni-bochum.de` (Christiane Helzel),  
`rossmani@math.wisc.edu` (James A. Rossmanith), `Bertram.Taetz@rub.de` (Bertram Taetz)

<sup>1</sup>Corresponding author

## 1. Introduction

The ideal magnetohydrodynamic (MHD) equations are a common model for the macroscopic behavior of collisionless plasma [8, 15, 21]. These equations model the fluid dynamics of an interacting mixture of positively and negatively charged particles, where each species is assumed to behave as a charged ideal gas. Under the MHD assumption, this mixture is taken to be quasi-neutral, meaning that as one species moves, the other reacts instantaneously. This assumption allows one to collapse what should be two sets of evolution equation into a single set of equations for the total mass, momentum, and energy of the mixture. Furthermore, the resulting dynamics are assumed to happen on slow time scales compared to the propagation time of light waves, which yields a simplified set of Maxwell equations.

All of the above described simplifications conspire to turn the original two-fluid plasma model into a system which can be viewed as a modified version of the compressible Euler equations from gas dynamics. In particular, the ideal MHD system can be written as a system of hyperbolic conservation laws, where the conserved quantities are mass, momentum, energy, and magnetic field. Furthermore, this system is equipped, just as the compressible Euler equations are, with an entropy inequality that features a convex scalar entropy and a corresponding entropy flux. Indeed, the scalar entropy, with some help from the fact that the magnetic field is divergence-free, can be used to define entropy variables in which the MHD system is in symmetric hyperbolic form [5, 14].

As has been noted many times in the literature (e.g., Brackbill and Barnes [6], Evans and Hawley [12], and Tóth [30]), numerical methods for ideal MHD must in general satisfy some discrete version of the divergence-free condition on the magnetic field:

$$\nabla \cdot \mathbf{B} = 0.$$

Failure to accomplish this generically leads to a nonlinear numerical instability, which often leads to negative pressures and/or densities. Starting with the paper of Brackbill and Barnes [6] in 1980, several approaches for controlling errors in  $\nabla \cdot \mathbf{B}$  have been proposed. An in-depth review of many of these methods can be found in Tóth [30]. We very briefly summarize the main points below.

**Projection methods.** A projection method was first used in the MHD context in the short paper of Brackbill and Barnes [6]. Various projection methods for use in conjunction with modern finite volume methods can be found in Tóth [30] and Balsara and Kim [3]. The basic approach can be viewed as a predictor-corrector method, whereby some standard finite volume or finite difference method is used to predict a magnetic field,  $\mathbf{B}^*$ , and then an elliptic equation is solved to project this predicted magnetic field to its (approximately) divergence-free subspace.

This method is attractive for it allows a variety of methods to be used in the prediction step, and then only requires one Poisson solve per time-step to correct it. The clear disadvantage of this approach is that it requires a global elliptic solve on a problem, ideal MHD, that is purely

hyperbolic. This could be especially computationally inefficient in the case of adaptively refined grids.

**Hyperbolic divergence cleaning methods.** This method was introduced by Dedner et al. [11], and is a close cousin to the above described projection method. The basic idea is to again solve for the divergence-error in the magnetic field. Instead of solving an elliptic equation, however, a damped hyperbolic equation is prescribed for the divergence error. This does not produce an exact divergence-free magnetic field; however, it allows for the divergence-error to be propagated and damped away from where it originated. The main advantage of this method is that it is easy to implement and requires no elliptic solve. The main disadvantage is that this approach has two tunable parameters: the speed of propagation of the error and the rate at which the divergence-error is damped. This is again problematic for adaptive mesh refinement, since different grid patches may need different parameter choices.

**Constrained transport methods.** The constrained transport (CT) approach for ideal MHD was introduced by Evans and Hawley [12]. The method is a modification of Yee's method [31] for electromagnetic wave propagation, and, at least in its original formulation, introduced staggered magnetic and electric fields. Since the introduction of the CT framework, several variants and modifications have been introduced, including the work of Balsara [2], Balsara and Spicer [4], Dai and Woodward [10], Fey and Torrilhon [13], Londrillo and Del Zanna [20], Rossmannith [25], Ryu et al. [26], and De Sterck [27]. An overview of many of these approaches, as well as the introduction of a few more variants, can be found in Tóth [30]. In particular, Tóth [30] showed that a staggered magnetic field is not necessary.

The CT framework, at least several versions of it, can also be viewed as a kind of predictor-corrector approach for the magnetic field. Roughly speaking, the idea is to again compute all of the conserved quantities with a standard finite volume method. From these computed quantities one then constructs an approximation to the electric field through the ideal Ohm's law. This electric field can then be used to update the magnetic vector potential, which in turn, can be used to compute a divergence-free magnetic field (see §3 for more details).

The main advantages of this approach are that (1) there is no elliptic solve and (2) there are no free parameters to choose such as in the hyperbolic divergence-cleaning technique.

We focus in this work on developing a constrained transport method for the 3D ideal MHD equations that is based on a high-resolution wave propagation scheme. Our proposed scheme is the 3D extension of the 2D scheme developed by Rossmannith [25], and is based on the high-resolution wave propagation method of Langseth and LeVeque [16]. In particular, in our extension we take great care to maintain the three most important properties of the 2D scheme:

1. All quantities, including all components of the magnetic field and magnetic potential, are treated as cell-centered;
2. We develop a high-resolution wave propagation scheme for evolving the magnetic potential; and
3. We develop a wave limiting approach that is applied during the vector potential evolution, which controls unphysical oscillations in the magnetic field.

After briefly reviewing the MHD equations in §2, we describe an overview of our proposed method in §3. One important issue that arises from this approach is the gauge choice; we discuss several possible choices in §4. Under the gauge condition that we choose, the 3D transport equation that must be solved for the magnetic potential is only weakly hyperbolic. We describe in detail in §5 how to numerically handle this difficulty. The resulting scheme is applied to several numerical test cases in §6.

## 2. Basic equations

The ideal magnetohydrodynamic (MHD) equations are a classical model from plasma physics that describe the macroscopic evolution of a quasi-neutral two-fluid plasma system. Under the quasi-neutral assumption, the two-fluid equations can be collapsed into a single set of fluid equations for the total mass, momentum, and energy of the system. The resulting equations can be written in the following form:

$$\frac{\partial}{\partial t} \begin{bmatrix} \rho \\ \rho\mathbf{u} \\ \mathcal{E} \\ \mathbf{B} \end{bmatrix} + \nabla \cdot \begin{bmatrix} \rho \\ \rho\mathbf{u} \\ \mathcal{E} + (p + \frac{1}{2}\|\mathbf{B}\|^2)\mathbb{I} - \mathbf{B}\mathbf{B} \\ \mathbf{u}(\mathcal{E} + p + \frac{1}{2}\|\mathbf{B}\|^2) - \mathbf{B}(\mathbf{u} \cdot \mathbf{B}) \\ \mathbf{u}\mathbf{B} - \mathbf{B}\mathbf{u} \end{bmatrix} = 0, \quad (1)$$

$$\nabla \cdot \mathbf{B} = 0, \quad (2)$$

where  $\rho$ ,  $\rho\mathbf{u}$ , and  $\mathcal{E}$  are the total mass, momentum, and energy densities of the plasma system, and  $\mathbf{B}$  is the magnetic field. The thermal pressure,  $p$ , is related to the conserved quantities through the ideal gas law:

$$p = (\gamma - 1) \left( \mathcal{E} - \frac{1}{2}\|\mathbf{B}\|^2 - \frac{1}{2}\rho\|\mathbf{u}\|^2 \right), \quad (3)$$

where  $\gamma = 5/3$  is the ideal gas constant.

The equation for the magnetic field comes from Faraday's law:

$$\mathbf{B}_{,t} + \nabla \times \mathbf{E} = 0, \quad (4)$$

where the electric field,  $\mathbf{E}$ , is approximated by Ohm's law for a perfect conductor:

$$\mathbf{E} = \mathbf{B} \times \mathbf{u}. \quad (5)$$

Under the Ohm's law assumption, we can rewrite Faraday's law in the following divergence form:

$$\mathbf{B}_{,t} + \nabla \times (\mathbf{B} \times \mathbf{u}) = \mathbf{B}_{,t} + \nabla \cdot (\mathbf{uB} - \mathbf{Bu}) = 0. \quad (6)$$

Since the electric field is determined entirely from Ohm's law, we do not require an evolution equation for it; and thus, the only other piece that we need from Maxwell's equations is the divergence-free condition on the magnetic field (2). A complete derivation and discussion of MHD system (1)-(2) can be found in several standard plasma physics textbooks (e.g., [8, 15, 21]).

### 2.1. $\nabla \cdot \mathbf{B} = 0$ is an involution

We first note that system (1), along with the equation of state equation (3), provides a full set of equations for the time evolution of all eight state variables:  $(\rho, \rho\mathbf{u}, \mathcal{E}, \mathbf{B})$ . These evolution equations form a hyperbolic system. In particular, the eigenvalues of the flux Jacobian in some arbitrary direction  $\mathbf{n}$  ( $\|\mathbf{n}\| = 1$ ) can be written as follows:

$$\begin{aligned} \lambda^{1,8} &= \mathbf{u} \cdot \mathbf{n} \mp c_f : \text{fast magnetosonic waves,} \\ \lambda^{2,7} &= \mathbf{u} \cdot \mathbf{n} \mp c_a : \text{Alfvén waves,} \\ \lambda^{3,6} &= \mathbf{u} \cdot \mathbf{n} \mp c_s : \text{slow magnetosonic waves,} \\ \lambda^4 &= \mathbf{u} \cdot \mathbf{n} : \text{entropy wave,} \\ \lambda^5 &= \mathbf{u} \cdot \mathbf{n} : \text{divergence wave,} \end{aligned}$$

where

$$\begin{aligned} a &\equiv \sqrt{\frac{\gamma p}{\rho}}, \\ c_a &\equiv \sqrt{\frac{(\mathbf{B} \cdot \mathbf{n})^2}{\rho}}, \\ c_f &\equiv \left\{ \frac{1}{2} \left[ a^2 + \frac{\|\mathbf{B}\|^2}{\rho} + \sqrt{\left( a^2 + \frac{\|\mathbf{B}\|^2}{\rho} \right)^2 - 4a^2 \frac{(\mathbf{B} \cdot \mathbf{n})^2}{\rho}} \right] \right\}^{1/2}, \\ c_s &\equiv \left\{ \frac{1}{2} \left[ a^2 + \frac{\|\mathbf{B}\|^2}{\rho} - \sqrt{\left( a^2 + \frac{\|\mathbf{B}\|^2}{\rho} \right)^2 - 4a^2 \frac{(\mathbf{B} \cdot \mathbf{n})^2}{\rho}} \right] \right\}^{1/2}. \end{aligned}$$

The eigenvalues are well-ordered in the sense that

$$\lambda^1 \leq \lambda^2 \leq \lambda^3 \leq \lambda^4 \leq \lambda^5 \leq \lambda^6 \leq \lambda^7 \leq \lambda^8.$$

The fast and slow magnetosonic waves are genuinely nonlinear, while the remaining waves are linearly degenerate. Note that the so-called *divergence-wave* has been made to travel at the speed  $\mathbf{u} \cdot \mathbf{n}$ , thus restoring Galilean invariance, by adding to (1) a term proportional to  $\nabla \cdot \mathbf{B}$  [14, 23, 24].

The additional equation (2) is not needed in the time evolution of the conserved variables in the following sense:

If (2) is true at some time  $t = T$ , then evolution equation (1) guarantees that (2) is true for all time.

This result follows from taking the divergence of Faraday's law, which yields:

$$\frac{\partial}{\partial t} (\nabla \cdot \mathbf{B}) = 0. \quad (7)$$

For this reason, (2) should not be regarded as *constraint* (such as the  $\nabla \cdot \mathbf{u} = 0$  constraint for the incompressible Navier-Stokes equations), but rather an *involution* [9].

## 2.2. The role of $\nabla \cdot \mathbf{B} = 0$ in numerical discretizations

Although  $\nabla \cdot \mathbf{B} = 0$  is an involution, and therefore has no dynamic impact on the evolution of the exact MHD system, the story is more complicated for numerical discretizations of ideal MHD. Brackbill and Barnes [6] gave a physical explanation as to why  $\nabla \cdot \mathbf{B} = 0$  should be satisfied in some appropriate discrete sense:

If  $\nabla \cdot \mathbf{B} \neq 0$ , then the magnetic force,

$$\mathbf{F} = \nabla \cdot \left\{ \mathbf{B} \mathbf{B} - \frac{1}{2} \|\mathbf{B}\|^2 \mathbb{I} \right\},$$

in the direction of the magnetic field, will not in general vanish:

$$\mathbf{F} \cdot \mathbf{B} = \|\mathbf{B}\|^2 (\nabla \cdot \mathbf{B}) \neq 0.$$

This spurious forcing can lead to numerical instabilities.

Another explanation as to why  $\nabla \cdot \mathbf{B} = 0$  should not be ignored in numerical discretizations of MHD, from a slightly different point-of-view, was offered by Barth [5]. Barth's explanation is based on the well-known result of Godunov [14] that the MHD entropy density,

$$U(q) = -\rho \log(p\rho^{-\gamma}),$$

produces a set of *entropy variables*,  $U_{,q}$ , that do not immediately symmetrize the ideal MHD equations. Instead, a symmetric hyperbolic form of ideal MHD can only be obtained if an additional term that is proportional to the divergence of the magnetic field is included in the MHD equations:

$$\underbrace{q_{,t} + \nabla \cdot \mathbf{F}(q)}_{\text{ideal MHD}} + \underbrace{\phi_{,q} \nabla \cdot \mathbf{B}}_{\text{additional term}} = 0, \quad \text{where } \phi(q) = (\gamma - 1) \frac{\rho \mathbf{u} \cdot \mathbf{B}}{p}.$$

By looking at how the entropy behaves on the discrete level, Barth [5] was able to prove that certain discontinuous Galerkin discretizations of the ideal MHD equations could be made to be *entropy stable* (see Tadmor [29]) if the discrete magnetic field were made globally divergence-free. The implication of this result is that schemes that do not control errors in the divergence of the magnetic field run the risk of becoming entropy unstable.

### 3. An unstaggered constrained transport framework

The main focus of this work is to extend the two-dimensional constrained transport method introduced by Rossmanith [25]. In this section we outline the basic framework of this approach. Each time step in the constrained transport algorithm has several sub-steps, which can be summarized as follows:

**Step 0.** Start with the current state:  $(\rho^n, \mathbf{u}^n, \mathcal{E}^n, \mathbf{B}^n, \mathbb{A}^n)$ .

**Step 1.** Update MHD variables via a standard finite volume scheme:

$$(\rho^n, \mathbf{u}^n, \mathcal{E}^n, \mathbf{B}^n) \implies (\rho^{n+1}, \mathbf{u}^{n+1}, \mathcal{E}^*, \mathbf{B}^*) .$$

**Step 2.** Define the time-averaged velocity:  $\mathbf{u}^{n+\frac{1}{2}} = \frac{1}{2} (\mathbf{u}^n + \mathbf{u}^{n+1})$ .

**Step 3.** Using the above calculated velocity,  $\mathbf{u}^{n+\frac{1}{2}}$ , solve the vector potential equation:

$$\mathbb{A}_{,t} + (\nabla \times \mathbb{A}) \times \mathbf{u}^{n+\frac{1}{2}} = -\nabla \phi.$$

This updates the vector potential:  $\mathbb{A}^n \implies \mathbb{A}^{n+1}$ .

**Step 4.** Compute the new magnetic field from the curl of the vector potential:

$$[B^1]_{ij}^{n+1} = \frac{[\mathbb{A}^3]_{i,j+1,k}^{n+1} - [\mathbb{A}^3]_{i,j-1,k}^{n+1}}{2\Delta y} - \frac{[\mathbb{A}^2]_{i,j,k+1}^{n+1} - [\mathbb{A}^2]_{i,j,k-1}^{n+1}}{2\Delta z}, \quad (8)$$

$$[B^2]_{ij}^{n+1} = \frac{[\mathbb{A}^1]_{i,j,k+1}^{n+1} - [\mathbb{A}^1]_{i,j,k-1}^{n+1}}{2\Delta z} - \frac{[\mathbb{A}^3]_{i+1,j,k}^{n+1} - [\mathbb{A}^3]_{i-1,j,k}^{n+1}}{2\Delta x}, \quad (9)$$

$$[B^3]_{ij}^{n+1} = \frac{[\mathbb{A}^2]_{i+1,j,k}^{n+1} - [\mathbb{A}^2]_{i-1,j,k}^{n+1}}{2\Delta x} - \frac{[\mathbb{A}^1]_{i,j+1,k}^{n+1} - [\mathbb{A}^1]_{i,j-1,k}^{n+1}}{2\Delta y}. \quad (10)$$

**Step 5.** Set the new total energy density value:

**Option 1:** Conserve total energy:

$$\mathcal{E}^{n+1} = \mathcal{E}^*.$$

**Option 2:** Keep the pressure the same before and after the constrained transport step (this sometimes helps in preventing the pressure from becoming negative, although it sacrifices energy conservation):

$$\mathcal{E}^{n+1} = \mathcal{E}^* + \frac{1}{2} (\|\mathbf{B}^{n+1}\|^2 - \|\mathbf{B}^*\|^2).$$

The above described algorithm guarantees that at each time step, the following discrete divergence is identically zero:

$$\begin{aligned} [\nabla \cdot \mathbf{B}]_{ij}^{n+1} &= \frac{[B^1]_{i+1,j,k}^{n+1} - [B^1]_{i-1,j,k}^{n+1}}{2\Delta x} + \frac{[B^2]_{i,j+1,k}^{n+1} - [B^2]_{i,j-1,k}^{n+1}}{2\Delta y} \\ &+ \frac{[B^3]_{i,j,k+1}^{n+1} - [B^3]_{i,j,k-1}^{n+1}}{2\Delta z} = 0. \end{aligned} \quad (11)$$

## 4. Vector potential equations and gauge conditions

The key step in the constrained transport framework as outlined in the previous section is **Step 3**, which requires one to solve an evolution equation for the magnetic vector potential. One question that immediately arises: what should be chosen for the gauge condition? In this section we briefly discuss several gauge conditions and their consequences on the evolution of the magnetic vector potential.

The starting point for this discussion is induction equation:

$$\mathbf{B}_{,t} + \nabla \times (\mathbf{B} \times \mathbf{u}) = 0, \quad (12)$$

where, for the purposes of the algorithm outlined in §3, we take the velocity,  $\mathbf{u}$ , as a given function. We set  $\mathbf{B} = \nabla \times \mathbb{A}$  and rewrite (12) as

$$\nabla \times \{\mathbb{A}_{,t} + (\nabla \times \mathbb{A}) \times \mathbf{u}\} = 0 \implies \mathbb{A}_{,t} + (\nabla \times \mathbb{A}) \times \mathbf{u} = -\nabla \phi, \quad (13)$$

where  $\phi$  is an arbitrary scalar function. Different choices of  $\phi$  represent different *gauge condition* choices.

Before we explore various gauge conditions, however, it is worth pointing out that the situation in the pure two-dimensional case (let's say in the  $(x, y)$  plane) is much simpler. The only component of the magnetic vector potential that influences the evolution in this case is  $\mathbb{A}^3$  (i.e., the component of the potential that is perpendicular to the evolution plane); and furthermore, all gauge choices lead to the same equation:

$$\mathbb{A}_{,t}^3 + u^1 \mathbb{A}_{,x}^3 + u^2 \mathbb{A}_{,y}^3 = 0,$$

where  $\mathbb{A}^3$  is uniquely defined up to an additive constant.

### 4.1. Coulomb gauge

An obvious choice for the gauge is to take the vector magnetic potential to be solenoidal:

$$\nabla \cdot \mathbb{A} = 0, \quad (14)$$

resulting in the *Coulomb gauge*. We are now able to add  $-\mathbf{u} \nabla \cdot \mathbb{A}$  to the left-hand side of (13) and obtain an equation for the potential that is in symmetric hyperbolic form:

$$\begin{bmatrix} \mathbb{A}^1 \\ \mathbb{A}^2 \\ \mathbb{A}^3 \end{bmatrix}_{,t} + \begin{bmatrix} -u^1 & -u^2 & -u^3 \\ -u^2 & u^1 & 0 \\ -u^3 & 0 & u^1 \end{bmatrix} \begin{bmatrix} \mathbb{A}^1 \\ \mathbb{A}^2 \\ \mathbb{A}^3 \end{bmatrix}_{,x} + \begin{bmatrix} u^2 & -u^1 & 0 \\ -u^1 & -u^2 & -u^3 \\ 0 & -u^3 & u^2 \end{bmatrix} \begin{bmatrix} \mathbb{A}^1 \\ \mathbb{A}^2 \\ \mathbb{A}^3 \end{bmatrix}_{,y} + \begin{bmatrix} u^3 & 0 & -u^1 \\ 0 & u^3 & -u^2 \\ -u^1 & -u^2 & -u^3 \end{bmatrix} \begin{bmatrix} \mathbb{A}^1 \\ \mathbb{A}^2 \\ \mathbb{A}^3 \end{bmatrix}_{,z} = - \begin{bmatrix} \phi_{,x} \\ \phi_{,y} \\ \phi_{,z} \end{bmatrix}. \quad (15)$$

The main difficulty with this approach, however, is that at each time step one must solve a Poisson equation to determine the Lagrange multiplier  $\phi$ :

$$-\nabla^2 \phi = \nabla \cdot [(\nabla \times \mathbb{A}) \times \mathbf{u}]. \quad (16)$$

Having to solve an elliptic equation in each time step makes this approach have the same efficiency problems as the projection method.

#### 4.2. Lorentz-like gauge

In the ideal MHD setting, since the speed of light is taken to be infinite, the Lorentz and Coulomb gauges are equivalent. However, one possibility is introduce a fictitious wave speed,  $\xi$ , that is larger than all other wave speeds in the MHD system. We can then take

$$\phi_{,t} = \xi^2 \nabla \cdot \mathbb{A}, \quad (17)$$

which results in the following evolution equation for  $(\mathbb{A}, \phi)$ :

$$\begin{bmatrix} \mathbb{A}^1 \\ \mathbb{A}^2 \\ \mathbb{A}^3 \\ \phi \end{bmatrix}_{,t} + \begin{bmatrix} 0 & -u^2 & -u^3 & 1 \\ 0 & u^1 & 0 & 0 \\ 0 & 0 & u^1 & 0 \\ \xi^2 & 0 & 0 & 0 \end{bmatrix} \begin{bmatrix} \mathbb{A}^1 \\ \mathbb{A}^2 \\ \mathbb{A}^3 \\ \phi \end{bmatrix}_{,x} + \begin{bmatrix} u^2 & 0 & 0 & 0 \\ -u^1 & 0 & -u^3 & 1 \\ 0 & 0 & u^2 & 0 \\ 0 & \xi^2 & 0 & 0 \end{bmatrix} \begin{bmatrix} \mathbb{A}^1 \\ \mathbb{A}^2 \\ \mathbb{A}^3 \\ \phi \end{bmatrix}_{,y} \quad (18)$$

$$+ \begin{bmatrix} u^3 & 0 & 0 & 0 \\ 0 & u^3 & 0 & 0 \\ -u^1 & -u^2 & 0 & 1 \\ 0 & 0 & \xi^2 & 0 \end{bmatrix} \begin{bmatrix} \mathbb{A}^1 \\ \mathbb{A}^2 \\ \mathbb{A}^3 \\ \phi \end{bmatrix}_{,z} = 0.$$

The flux Jacobian of this system in some direction  $\mathbf{n}$  (where  $\|\mathbf{n}\| = 1$ ) can be written as

$$N(\mathbf{n}) = \begin{bmatrix} n^2 u^2 + n^3 u^3 & -n^1 u^2 & -n^1 u^3 & n^1 \\ -n^2 u^1 & n^1 u^1 + n^3 u^3 & -n^2 u^3 & n^2 \\ -n^3 u^1 & -n^3 u^2 & n^1 u^1 + n^2 u^2 & n^3 \\ n^1 \xi^2 & n^2 \xi^2 & n^3 \xi^2 & 0 \end{bmatrix}. \quad (19)$$

The eigenvalues of this matrix are

$$\lambda = \{-\xi, \xi, \mathbf{u} \cdot \mathbf{n}, \mathbf{u} \cdot \mathbf{n}\}. \quad (20)$$

If  $\xi > |\mathbf{u} \cdot \mathbf{n}|$ , the right-eigenvectors of  $N(\mathbf{n})$  are complete, and thus, the system is hyperbolic.

Although this seems like a potentially useful gauge choice, we found in practice that numerical solutions to system (18) did not produce accurate magnetic fields. In particular, we observed errors in the location of strong shocks, which is presumably due to the fact that on the discrete level

$$\nabla \times \nabla \phi \neq 0,$$

thus resulting in errors in  $\mathbf{B}$ .

### 4.3. Helicity-inspired gauge

Another gauge possibility is to directly set the scalar function,  $\phi$ , to something useful. One such choice is

$$\phi = \mathbf{u} \cdot \mathbf{A}, \quad (21)$$

which is inspired by the magnetic helicity:  $\mathbf{B} \cdot \mathbf{A}$ . This yields the system:

$$\mathbb{A}_{,t} + u^1 \mathbb{A}_{,x} + u^2 \mathbb{A}_{,y} + u^3 \mathbb{A}_{,z} = M \mathbb{A}, \quad (22)$$

where

$$M := - \begin{bmatrix} u_{,x}^1 & u_{,x}^2 & u_{,x}^3 \\ u_{,y}^1 & u_{,y}^2 & u_{,y}^3 \\ u_{,z}^1 & u_{,z}^2 & u_{,z}^3 \end{bmatrix}. \quad (23)$$

One obvious approach for solving this equation is via operator splitting, whereby equation (22) is split into three decoupled advection equations:

$$\mathbb{A}_{,t} + u^1 \mathbb{A}_{,x} + u^2 \mathbb{A}_{,y} + u^3 \mathbb{A}_{,z} = 0, \quad (24)$$

and a ‘linear’ ordinary differential equation<sup>2</sup>:

$$\mathbb{A}_{,t} = M \mathbb{A}. \quad (25)$$

The main difficulty with this approach is that the matrix  $M$  in equation (25) could (and often does) have eigenvalues that have a positive real part; thereby, causing this system to be inherently unstable. For this reason, numerical tests using this gauge condition were generally not successful.

### 4.4. Weyl gauge

The choice that we finally settled on was the simple gauge:

$$\phi = 0. \quad (26)$$

In this approach, the resulting evolution equation is simply (13) with a zero right-hand side.

As we will describe in detail in the next section, §5, the resulting system is only *weakly* hyperbolic. This is due to the fact that there are certain directions in which the matrix of right-eigenvectors of the flux Jacobian does not have full rank. This degeneracy causes some numerical difficulties, which we were able to overcome through the creation of a modified wave propagation scheme. The details of this approach are described in the next section.

---

<sup>2</sup>This equation is linear in the sense that the velocity,  $\mathbf{u}$ , is taken to be frozen in time at  $t = t^{n+1/2}$ .

## 5. Numerical methods

### 5.1. The wave propagation scheme of Langseth and LeVeque [16]

In **Step 1** of the constrained transport method (compare with §3) we apply a numerical method for the three-dimensional MHD equations. Here we use a version of the three-dimensional wave propagation algorithm of Langseth and LeVeque [16], see also [17], which is based on a decomposition of flux differences at grid cell interfaces as outlined in [1]. This is a multidimensional high-resolution finite volume method which is second order accurate for smooth solutions and which leads to an accurate capturing of shock waves.

To outline the main steps of this algorithm, we consider a three-dimensional hyperbolic system of the general form

$$\mathbf{q}_{,t} + \mathbf{f}(\mathbf{q})_{,x} + \mathbf{g}(\mathbf{q})_{,y} + \mathbf{h}(\mathbf{q})_{,z} = \mathbf{0}, \quad (27)$$

with  $\mathbf{q} : \mathbb{R}^3 \times \mathbb{R}^+ \rightarrow \mathbb{R}^m$  and  $\mathbf{f}, \mathbf{g}, \mathbf{h} : \mathbb{R}^m \rightarrow \mathbb{R}^m$ . In quasilinear form the system reads

$$\mathbf{q}_{,t} + A(\mathbf{q})\mathbf{q}_{,x} + B(\mathbf{q})\mathbf{q}_{,y} + C(\mathbf{q})\mathbf{q}_{,z} = \mathbf{0}. \quad (28)$$

Let  $Q_{i,j,k}^n$  denote the cell average of the conserved quantity  $\mathbf{q}$  in grid cell  $(i, j, k)$  of a Cartesian mesh. The numerical method can be written in the form

$$\begin{aligned} Q_{i,j,k}^{n+1} = & Q_{i,j,k}^n - \frac{\Delta t}{\Delta x} \left( \mathcal{A}^+ \Delta Q_{i-\frac{1}{2},j,k} + \mathcal{A}^- \Delta Q_{i+\frac{1}{2},j,k} \right) \\ & - \frac{\Delta t}{\Delta y} \left( \mathcal{B}^+ \Delta Q_{i,j-\frac{1}{2},k} + \mathcal{B}^- \Delta Q_{i,j+\frac{1}{2},k} \right) \\ & - \frac{\Delta t}{\Delta z} \left( \mathcal{C}^+ \Delta Q_{i,j,k-\frac{1}{2}} + \mathcal{C}^- \Delta Q_{i,j,k+\frac{1}{2}} \right) \\ & - \frac{\Delta t}{\Delta x} \left( \tilde{F}_{i+\frac{1}{2},j,k} - \tilde{F}_{i-\frac{1}{2},j,k} \right) - \frac{\Delta t}{\Delta y} \left( \tilde{G}_{i,j+\frac{1}{2},k} - \tilde{G}_{i,j-\frac{1}{2},k} \right) \\ & - \frac{\Delta t}{\Delta z} \left( \tilde{H}_{i,j,k+\frac{1}{2}} - \tilde{H}_{i,j,k-\frac{1}{2}} \right). \end{aligned} \quad (29)$$

The first three lines in (29) describe a first order accurate update and the last two lines represent higher order correction terms. The wave propagation method is a so-called truly multidimensional scheme in the sense that no dimensional splitting is used to approximate the mixed derivative terms that are required in a second order accurate update.

At each grid cell interface in the  $x$ -direction, we decompose the flux differences

$$\Delta F_{i-\frac{1}{2},j,k} = \mathbf{f}(Q_{i,j,k}^n) - \mathbf{f}(Q_{i-1,j,k}) \quad (30)$$

into waves

$$\mathcal{Z}_{i-\frac{1}{2},j,k}^p = \left[ \ell_{i-\frac{1}{2},j,k}^p \cdot \Delta F_{i-\frac{1}{2},j,k} \right] r_{i-\frac{1}{2},j,k}^p, \quad (31)$$

which are moving with speeds  $s_{i-\frac{1}{2},j,k}^p$ ,  $p = 1, \dots, M_w$ . For this decomposition, we use the left and right eigenvectors proposed by Powell et al. [24] for a linearized flux Jacobian matrix of the MHD equations. The fluctuations used in

the first order update have the form:

$$\begin{aligned}\mathcal{A}^+ \Delta Q_{i-\frac{1}{2},j,k} &= \sum_{p: s_{i-\frac{1}{2},j,k}^p > 0} \mathcal{Z}_{i-\frac{1}{2},j,k}^p + \frac{1}{2} \sum_{p: s_{i-\frac{1}{2},j,k}^p = 0} \mathcal{Z}_{i-\frac{1}{2},j,k}^p, \\ \mathcal{A}^- \Delta Q_{i-\frac{1}{2},j,k} &= \sum_{p: s_{i-\frac{1}{2},j,k}^p < 0} \mathcal{Z}_{i-\frac{1}{2},j,k}^p + \frac{1}{2} \sum_{p: s_{i-\frac{1}{2},j,k}^p = 0} \mathcal{Z}_{i-\frac{1}{2},j,k}^p.\end{aligned}\quad (32)$$

Analogously, we compute fluctuations in the  $y$  and the  $z$  direction. An advantage of the decomposition of the flux differences compared to the standard wave propagation method from [16, 18], which is based on an eigenvector decomposition of the jumps of the conserved quantities at each grid cell interface, is that the local linearization of the flux Jacobian matrix does not require Roe averages which are quite difficult to compute for the MHD equations [7]. Here we used a simple arithmetic averaging instead.

The waves and speeds are also used to compute high-resolution correction terms which are added in the update (29) in flux difference form. For the waves in the  $x$ -direction, they have the form

$$\tilde{F}_{i-\frac{1}{2},j,k} = \frac{1}{2} \sum_{p=1}^{M_w} \text{sign}(s_{i-\frac{1}{2},j,k}^p) \left( 1 - \frac{\Delta t}{\Delta x} |s_{i-\frac{1}{2},j,k}^p| \right) \mathcal{Z}_{i-\frac{1}{2},j,k}^p \phi_{i-\frac{1}{2},j,k}(\theta_{i-\frac{1}{2},j,k}^p), \quad (33)$$

where

$$\theta_{i-\frac{1}{2},j,k}^p := \frac{\mathcal{Z}_{i-\frac{1}{2},j,k}^p \cdot \mathcal{Z}_{I-\frac{1}{2},j,k}^p}{\mathcal{Z}_{i-\frac{1}{2},j,k}^p \cdot \mathcal{Z}_{i-\frac{1}{2},j,k}^p}, \quad \text{where } I = \begin{cases} i-1 & \text{if } s_{i-\frac{1}{2},j,k}^p > 0 \\ i+1 & \text{if } s_{i-\frac{1}{2},j,k}^p < 0 \end{cases},$$

is a measure of the location smoothness in the  $p$ -th wave family and  $\phi(\theta)$  is a total variation diminishing (TVD) limiter function [18, 28].

The wave propagation method is a 1-step, unsplit, second-order accurate method in both space and time (for smooth solutions); and therefore, is based on a Taylor series expansions in time:

$$\begin{aligned}q(t + \Delta t, \mathbf{x}) &= q + \Delta t q_{,t} + \frac{1}{2} \Delta t^2 q_{,tt} + \mathcal{O}(\Delta t^3) \\ &= q - \Delta t \left[ f_{,x} + g_{,y} + h_{,z} \right] + \frac{1}{2} \Delta t^2 \left\{ (Af_{,x})_{,x} + (Bg_{,y})_{,y} + (Ch_{,z})_{,z} \right. \\ &\quad \left. + \underbrace{(Ag_{,y})_{,x} + (Ah_{,z})_{,x} + (Bf_{,x})_{,y} + (Bh_{,z})_{,y} + (Cf_{,x})_{,z} + (Cg_{,y})_{,z}}_{\text{Transverse terms}} \right\} + \mathcal{O}(\Delta t^3),\end{aligned}$$

where  $A$ ,  $B$ , and  $C$  are the flux Jacobians in each of the three Cartesian directions, and time derivatives have been replaced by spatial derivations through the conservation law. The wave propagation method as described so far, approximates each of the terms in the above Taylor series to second order accuracy, except those terms marked as *transverse terms*. The transverse terms

are approximated via additional Riemann solvers known as *transverse Riemann solvers*. Additionally, Langseth and LeVeque [16] found that in order to achieve optimal stability bounds, additional so-called *double transverse Riemann solvers* are required to approximate certain mixed third-derivative terms. We omit a full discussion of the transverse and double transverse terms in this work, and instead, refer the reader to the paper of Langseth and LeVeque [16].

### 5.2. The evolution of the magnetic potential

We now describe a numerical method for the evolution equation of the magnetic potential using the Weyl gauge, i.e. for the discretization of (13) with zero right hand side. The equation can be written in the form

$$\mathbb{A}_{,t} + N_1(\mathbf{u}) \mathbb{A}_{,x} + N_2(\mathbf{u}) \mathbb{A}_{,y} + N_3(\mathbf{u}) \mathbb{A}_{,z} = 0, \quad (34)$$

with

$$N_1 = \begin{bmatrix} 0 & -u^2 & -u^3 \\ 0 & u^1 & 0 \\ 0 & 0 & u^1 \end{bmatrix}, \quad N_2 = \begin{bmatrix} u^2 & 0 & 0 \\ -u^1 & 0 & -u^3 \\ 0 & 0 & u^2 \end{bmatrix}, \quad N_3 = \begin{bmatrix} u^3 & 0 & 0 \\ 0 & u^3 & 0 \\ -u^1 & -u^2 & 0 \end{bmatrix}. \quad (35)$$

#### 5.2.1. Weak hyperbolicity

The system (34) is hyperbolic, if for any direction  $\mathbf{n} \in S^2$  the matrix

$$n^1 N_1 + n^2 N_2 + n^3 N_3 = \begin{bmatrix} n^2 u^2 + n^3 u^3 & -n^1 u^2 & -n^1 u^3 \\ -n^2 u^1 & n^1 u^1 + n^3 u^3 & -n^2 u^3 \\ -n^3 u^1 & -n^3 u^2 & n^1 u^1 + n^2 u^2 \end{bmatrix}$$

is diagonalizable with real eigenvalues. The eigenvalues are

$$\lambda = \{0, \mathbf{n} \cdot \mathbf{u}, \mathbf{n} \cdot \mathbf{u}\}; \quad (36)$$

and therefore, we always have real eigenvalues. The eigenvectors can be written in the following form:

$$R = \begin{bmatrix} r^{(1)} & | & r^{(2)} & | & r^{(3)} \end{bmatrix} = \begin{bmatrix} n^1 & n^2 u^3 - n^3 u^2 & u^1 (\mathbf{n} \cdot \mathbf{u}) - n^1 \|\mathbf{u}\|^2 \\ n^2 & n^3 u^1 - n^1 u^3 & u^2 (\mathbf{n} \cdot \mathbf{u}) - n^2 \|\mathbf{u}\|^2 \\ n^3 & n^1 u^2 - n^2 u^1 & u^3 (\mathbf{n} \cdot \mathbf{u}) - n^3 \|\mathbf{u}\|^2 \end{bmatrix}. \quad (37)$$

Assuming that  $\|\mathbf{u}\| \neq 0$  and  $\|\mathbf{n}\| = 1$ , the determinant of matrix  $R$  can be written as

$$\det(R) = -\|\mathbf{u}\|^3 \cos(\alpha) \sin^2(\alpha), \quad (38)$$

where  $\alpha$  is the angle between the vectors  $\mathbf{n}$  and  $\mathbf{u}$ . The difficulty is that for any non-zero velocity vector,  $\mathbf{u}$ , one can always find four directions,  $\alpha = 0, \pi/2, \pi$ , and  $3\pi/2$ , such that  $\det(R) = 0$ . In other words, for every  $\|\mathbf{u}\| \neq 0$  there exists four degenerate directions in which the eigenvectors are incomplete. Therefore, system (34)–(35) is only *weakly hyperbolic*.

### 5.2.2. An example: the difficulty with weakly hyperbolic systems

The application of standard methods for hyperbolic systems can lead to singularities when two eigenvectors coincide. Typically, finite volume methods for hyperbolic equations are based on an eigenvector decomposition (using eigenvectors of the flux Jacobian matrix) of the jump of the quantity  $\mathbf{A}$  in the direction normal to the grid cell interface (and possibly also tangential directions).

We illustrate this point with the following simple example:

$$\begin{bmatrix} u \\ v \end{bmatrix}_{,t} + \begin{bmatrix} -\varepsilon & 1 \\ 0 & \varepsilon \end{bmatrix} \begin{bmatrix} u \\ v \end{bmatrix}_{,x} = 0, \quad (39)$$

where  $\varepsilon \in \mathbb{R}$  is a constant. The eigen-decomposition of the flux Jacobian can be written as follows:

$$\begin{bmatrix} -\varepsilon & 1 \\ 0 & \varepsilon \end{bmatrix} = R \Lambda R^{-1} = \begin{bmatrix} 1 & 1 \\ 0 & 2\varepsilon \end{bmatrix} \cdot \begin{bmatrix} -\varepsilon & 0 \\ 0 & \varepsilon \end{bmatrix} \cdot \frac{1}{2\varepsilon} \begin{bmatrix} 2\varepsilon & -1 \\ 0 & 1 \end{bmatrix}. \quad (40)$$

Since the eigenvalues are always real, this system is hyperbolic. For all  $\varepsilon \neq 0$ , the system is strongly hyperbolic, and for  $\varepsilon = 0$  the system is only weakly hyperbolic. Since we have the exact eigen-decomposition, we can write down the exact solution for the Cauchy problem for all  $\varepsilon$ :

$$\begin{bmatrix} u \\ v \end{bmatrix} = \begin{bmatrix} u_0(x + \varepsilon t) - \frac{1}{2\varepsilon} \{v_0(x + \varepsilon t) - v_0(x - \varepsilon t)\} \\ v_0(x - \varepsilon t) \end{bmatrix}. \quad (41)$$

In the weakly hyperbolic limit we obtain:

$$\lim_{\varepsilon \rightarrow 0} \begin{bmatrix} u \\ v \end{bmatrix} = \begin{bmatrix} u_0(x) - t v'_0(x) \\ v_0(x) \end{bmatrix}. \quad (42)$$

The change in dynamics between the strongly and weakly hyperbolic regimes is quite dramatic: in the strongly hyperbolic case the total energy is conserved, while in the weakly hyperbolic case the amplitude of the solution growth linearly in time.

### 5.2.3. An operator split approach

In the case of the magnetic vector potential equation (34)-(35), the weak hyperbolicity is only an artifact of how we are evolving the magnetic potential. One should remember that the underlying equations (i.e., the ideal MHD system) are in fact hyperbolic. One way to understand all of this is to remember that the true velocity field,  $\mathbf{u}$ , depends on the magnetic potential in a nonlinear wave. That is, even though there might be instantaneous *growth* in the vector potential due to the weak hyperbolicity in the potential equation, this growth will immediately change the velocity field in such a way so that the overall system remains hyperbolic.

Numerically, however, we must construct a modified finite volume method that can handle this *short-lived* weak hyperbolicity. Through some experimentation with various ideas, we found that simple operator splitting techniques

lead to robust numerical methods. In particular, we found that there are two obvious ways to split system (13) into sub-problems.

The first possibility is based on a decomposition of the form

$$\begin{aligned}
\text{Sub-problem 1:} \quad & \mathbb{A}_{,t}^1 + u^2 \mathbb{A}_{,y}^1 + u^3 \mathbb{A}_{,z}^1 = 0, \\
& \mathbb{A}_{,t}^2 - u^1 \mathbb{A}_{,y}^1 = 0, \\
& \mathbb{A}_{,t}^3 - u^1 \mathbb{A}_{,z}^1 = 0, \\
\text{Sub-problem 2:} \quad & \mathbb{A}_{,t}^1 - u^2 \mathbb{A}_{,x}^2 = 0, \\
& \mathbb{A}_{,t}^2 + u^1 \mathbb{A}_{,x}^2 + u^3 \mathbb{A}_{,z}^2 = 0, \\
& \mathbb{A}_{,t}^3 - u^2 \mathbb{A}_{,z}^2 = 0, \\
\text{Sub-problem 3:} \quad & \mathbb{A}_{,t}^1 - u^3 \mathbb{A}_{,x}^3 = 0, \\
& \mathbb{A}_{,t}^2 - u^3 \mathbb{A}_{,y}^3 = 0, \\
& \mathbb{A}_{,t}^3 + u^1 \mathbb{A}_{,y}^3 + u^2 \mathbb{A}_{,x}^3 = 0.
\end{aligned} \tag{43}$$

Consider first sub-problem 1. The first equation can be approximated using the two-dimensional method described in [25, Section 5.3]. There, a modification of LeVeques wave propagation method was described which leads to a second order accurate approximation for smooth solutions while at the same time limiters were introduced which avoid oscillations in the magnetic potential as well as in the derivatives of the magnetic potential and thus in the magnetic field. Once the quantity  $\mathbb{A}^1$  is updated, simple finite difference approximations can be used to update  $\mathbb{A}^2$  and  $\mathbb{A}^3$ . The sub-problems 2 and 3 can be approached analogously and a Strang-type splitting can be used to approximate (34). We have tested this splitting and obtained very satisfying results.

A second approach to split (13) is based on dimension splitting, i.e. we consecutively solve the problems

$$\begin{aligned}
\text{Sub-problem 1:} \quad & \mathbb{A}_{,t}^1 - u^2 \mathbb{A}_{,x}^2 - u^3 \mathbb{A}_{,x}^3 = 0, \\
& \mathbb{A}_{,t}^2 + u^1 \mathbb{A}_{,x}^2 = 0, \\
& \mathbb{A}_{,t}^3 + u^1 \mathbb{A}_{,x}^3 = 0, \\
\text{Sub-problem 2:} \quad & \mathbb{A}_{,t}^1 + u^2 \mathbb{A}_{,y}^1 = 0, \\
& \mathbb{A}_{,t}^2 - u^1 \mathbb{A}_{,y}^1 - u^3 \mathbb{A}_{,y}^3 = 0, \\
& \mathbb{A}_{,t}^3 + u^2 \mathbb{A}_{,y}^3 = 0, \\
\text{Sub-problem 3:} \quad & \mathbb{A}_{,t}^1 + u^3 \mathbb{A}_{,z}^1 = 0, \\
& \mathbb{A}_{,t}^2 + u^3 \mathbb{A}_{,z}^2 = 0, \\
& \mathbb{A}_{,t}^3 - u^1 \mathbb{A}_{,z}^1 - u^2 \mathbb{A}_{,z}^2 = 0.
\end{aligned} \tag{44}$$

We will now present a numerical method which is based on this second splitting. Our method should be easy to adapt by other users in particular also by those who do not base their numerical method on the wave propagation algorithm.

We denote the numerical solution operator for sub-problem 1, 2 and 3 by  $L_1$ ,  $L_2$  and  $L_3$ , respectively. Then a Strang-type operator splitting method can be written in the form

$$(\mathbb{A})^{n+1} = L_1^{\Delta t/2} L_2^{\Delta t/2} L_3^{\Delta t} L_2^{\Delta t/2} L_1^{\Delta t/2} (\mathbb{A})^n.$$

One time step from  $t^n$  to  $t^{n+1}$  consists in consecutively solving sub-problem 1 over a half time step, sub-problem 2 over a half time step, sub-problem 3 over a full time step, sub-problem 2 over another half time step and finally solving sub-problem 1 over another half time step.

#### 5.2.4. Discretization of sub-problem 1

We now present the details for the approximation of the first sub-problem from (44) for a time step from  $\tau^n$  to  $\tau^{n+1}$ . The evolution of  $\mathbb{A}^2$  and  $\mathbb{A}^3$  is described by two decoupled scalar transport equations, which have the form

$$\begin{aligned} \partial_t \mathbb{A}^2(t, x, y, z) + u^1(\tau^{n+\frac{1}{2}}, x, y, z) \partial_x \mathbb{A}^2(t, x, y, z) &= 0, \\ \partial_t \mathbb{A}^3(t, x, y, z) + u^1(\tau^{n+\frac{1}{2}}, x, y, z) \partial_x \mathbb{A}^3(t, x, y, z) &= 0. \end{aligned} \quad (45)$$

We assume that cell average values of the quantity  $\mathbb{A}^{2,3}$  are given at time  $\tau^n$  and we wish to approximate  $\mathbb{A}^{2,3}$  at time  $\tau^{n+1}$ . In our application, cell centered values of the advection speed  $u^1$  are given at the intermediate time level (see **Step 2** of the algorithm from §3).

The update has for all  $i, j, k$  and  $l \in \{2, 3\}$  the form

$$\begin{aligned} (\mathbb{A}^l)_{ijk}^{n+1} &= (\mathbb{A}^l)_{ijk}^n - \frac{\Delta\tau}{\Delta x} \left[ \mathcal{A}^- \Delta \mathbb{A}_{i+\frac{1}{2},j,k}^l + \mathcal{A}^+ \Delta \mathbb{A}_{i-\frac{1}{2},j,k}^l \right] \\ &\quad - \frac{\Delta\tau}{\Delta x} \left[ \tilde{F}_{i+\frac{1}{2},j,k}^l - \tilde{F}_{i-\frac{1}{2},j,k}^l \right], \end{aligned} \quad (46)$$

with

$$\begin{aligned} \mathcal{W}_{i-\frac{1}{2},j,k}^l &:= (\mathbb{A}^l)_{i,j,k}^n - (\mathbb{A}^l)_{i-1,j,k}^n, \\ \mathcal{A}^- \Delta \mathbb{A}_{i-\frac{1}{2},j,k}^l &:= \min(u_{i-1,j,k}^1, 0) \mathcal{W}_{i-\frac{1}{2},j,k}^l, \\ \mathcal{A}^+ \Delta \mathbb{A}_{i-\frac{1}{2},j,k}^l &:= \max(u_{i,j,k}^1, 0) \mathcal{W}_{i-\frac{1}{2},j,k}^l, \end{aligned}$$

and

$$\begin{aligned} \tilde{F}_{i-\frac{1}{2},j,k}^l &:= \frac{1}{2} |u_{i-1,j,k}^1| \left( 1 - \frac{\Delta\tau}{\Delta x} \frac{u_{i-\frac{1}{2},j,k}^1}{|u_{i-1,j,k}^1|} u_{i-1,j,k}^1 \right) \mathcal{W}_{i-\frac{1}{2},j,k}^l \phi_{i-\frac{1}{2},j,k}, \\ \tilde{F}_{i+\frac{1}{2},j,k}^l &:= \frac{1}{2} |u_{i,j,k}^1| \left( 1 - \frac{\Delta\tau}{\Delta x} \frac{u_{i+\frac{1}{2},j,k}^1}{|u_{i,j,k}^1|} u_{i,j,k}^1 \right) \mathcal{W}_{i+\frac{1}{2},j,k}^l \phi_{i+\frac{1}{2},j,k}. \end{aligned}$$

Here  $u_{i,j,k}^1$  is a cell centered value and  $u_{i-\frac{1}{2},j,k}^1 = (u_{i-1,j,k}^1 + u_{i,j,k}^1)/2$  is a face centered value.

In order to avoid unphysical oscillations near discontinuities a limiter function  $\phi$  is used. This can be interpreted as wave limiter, i.e. the *wave*  $\mathcal{W}_{i-\frac{1}{2},j,k}$  is limited, compare with [17].

It is a well known problem that constrained transport methods can introduce unphysical oscillations in the magnetic field. In [25] an important modification of standard limiting techniques was introduced which is also used here. A method which has the TVD property for the quantity  $\mathbb{A}^{2,3}$  can be obtained by using a limiter of the form

$$\phi_{i-\frac{1}{2},j,k} = \phi \left( \frac{\mathcal{W}_{I-\frac{1}{2},j,k}^l}{\mathcal{W}_{i-\frac{1}{2},j,k}^l} \right),$$

where  $\phi$  is a standard limiter function and the index  $I$  is chosen in upwind direction based on the advection speed  $u_{i-\frac{1}{2},j,k}^1$ . In the constrained transport method,  $x$  derivatives of  $\mathbb{A}^{2,3}$  are used in the computation of the magnetic field via (9), (10). In order to avoid unphysical oscillations in the magnetic field the limiter is based on wave differences and has the form

$$\phi_{i-\frac{1}{2},j,k} = \phi \left( \frac{\Delta \mathcal{W}_{I,j,k}^l}{\Delta \mathcal{W}_{i,j,k}^l} \right).$$

Here  $\Delta \mathcal{W}_{i,j,k}^l = \mathcal{W}_{i+\frac{1}{2},j,k}^l - \mathcal{W}_{i-\frac{1}{2},j,k}^l$  and the index  $I$  is again chosen in upwind direction.

Once we have updated  $\mathbb{A}^2$  and  $\mathbb{A}^3$ , we update  $\mathbb{A}^1$  by discretizing the equation

$$\mathbb{A}_{,t}^1 - u^2 \mathbb{A}_{,x}^2 - u^3 \mathbb{A}_{,x}^3 = 0. \quad (47)$$

For this we use a finite difference method of the form

$$\begin{aligned} (\mathbb{A}^1)_{i,j,k}^{n+1} = & (\mathbb{A}^1)_{i,j,k}^n + \frac{\Delta \tau}{2} \left[ (u^2)_{i,j,k}^{n+\frac{1}{2}} \left( D_x(\mathbb{A}^2)_{i,j,k}^n + D_x(\mathbb{A}^2)_{i,j,k}^{n+1} \right) \right. \\ & \left. + (u^3)_{i,j,k}^{n+\frac{1}{2}} \left( D_x(\mathbb{A}^3)_{i,j,k}^n + D_x(\mathbb{A}^3)_{i,j,k}^{n+1} \right) \right], \end{aligned} \quad (48)$$

where  $D_x$  is the standard centered finite difference operator in the  $x$  direction, i.e.

$$D_x(\mathbb{A}^2)_{i,j,k}^n = \left( (\mathbb{A}^2)_{i+1,j,k}^n - (\mathbb{A}^2)_{i-1,j,k}^n \right) / (2\Delta x).$$

### 5.3. A diffusive limiter

For the spatially two-dimensional case, the limiting of wave differences eliminates unphysical oscillations in the magnetic field, see [25]. In the three-dimensional case, the equation for the magnetic potential is more challenging and only weakly hyperbolic. The numerical method is a combination of one-dimensional hyperbolic solvers and ode solvers. This complex update can introduce some oscillations in the magnetic potential and thus in the magnetic

field. In fact we have observed some oscillations in the magnetic field for the violent cloud-shock interaction problem discussed in §6.2.3.

To eliminate these oscillations we introduce a diffusive limiter which is inspired by the artificial viscosity method (e.g., [22]). Instead of (34), we discretize the problem with an added dissipative term

$$\mathbb{A}_{,t} + N_1(\mathbf{u})\mathbb{A}_{,x} + N_2(\mathbf{u})\mathbb{A}_{,y} + N_3(\mathbf{u})\mathbb{A}_{,z} = \nabla \cdot (\varepsilon \nabla \mathbb{A}), \quad (49)$$

where the parameter  $\varepsilon$  depends on the solution structure and controls the amount of artificial viscosity. We choose

$$\varepsilon = \nu \alpha h, \quad (50)$$

where  $\nu$  is a positive constant which will be discussed below,  $\alpha$  is a smoothness indicator which is close to zero in smooth regions and close to 0.5 near discontinuities and  $h$  indicates the mesh width.

We implement the diffusive limiter in each fractional step of our dimensional split approach. Consider again only the discretization used in the first substep of the splitting (44). Here we introduce an additional update which can be interpreted as an approximation of the diffusion equation

$$\mathbb{A}_{,t} = \nu \alpha \Delta x \mathbb{A}_{,xx}. \quad (51)$$

The simplest explicit treatment has for all  $i, j, k$  the form

$$\begin{aligned} \mathbb{A}_{i,j,k}^{n+1} &= \mathbb{A}_{i,j,k}^n + \Delta \tau \Delta x \nu \alpha \frac{\mathbb{A}_{i-1,j,k}^n - 2\mathbb{A}_{i,j,k}^n + \mathbb{A}_{i+1,j,k}^n}{\Delta x^2} \\ &= \mathbb{A}_{i,j,k}^n + \frac{\Delta \tau}{\Delta x} \nu \alpha (\mathbb{A}_{i-1,j,k}^n - 2\mathbb{A}_{i,j,k}^n + \mathbb{A}_{i+1,j,k}^n). \end{aligned} \quad (52)$$

Stability requires that

$$2\alpha \nu \Delta x \Delta \tau \leq \Delta x^2.$$

Thus we can add a diffusive limiter in the form of an explicit update for all components  $l \in \{1, 2, 3\}$  of the magnetic potential:

$$\tilde{\mathbb{A}}_{i,j,k}^l := \mathbb{A}_{i,j,k}^l + \tilde{\nu} \alpha (\mathbb{A}_{i-1,j,k}^l - 2\mathbb{A}_{i,j,k}^l + \mathbb{A}_{i+1,j,k}^l). \quad (53)$$

This update is stable provided that  $0 \leq \alpha \leq 1/2$  and  $\tilde{\nu} \leq 1$ .

The smoothness indicator  $\alpha$  was computed according to the formulas

$$\alpha = \max \left( \left| \frac{a_l}{a_l + a_r} - \frac{1}{2} \right|, \left| \frac{a_r}{a_l + a_r} - \frac{1}{2} \right| \right), \quad (54)$$

with

$$a_l = 1 / \left( \epsilon + (\mathbb{A}_{i,j,k}^l - \mathbb{A}_{i-1,j,k}^l)^2 \right)^2, \quad a_r = 1 / \left( \epsilon + (\mathbb{A}_{i+1,j,k}^l - \mathbb{A}_{i,j,k}^l)^2 \right)^2, \quad (55)$$

and  $\epsilon = 10^{-8}$ .

#### 5.4. Discretization of the 2.5 dimensional problem

In order to construct and analyse methods for the three-dimensional MHD equations, it is instructive to also look at the so-called 2.5 dimensional case. In this case we assume that  $\mathbf{u}$  and  $\mathbf{B}$  are three-dimensional vectors but all conserved quantities  $[\rho, \rho\mathbf{u}, \mathcal{E}, \mathbf{B}]^T$  are functions of only two spatial variables, say  $\mathbf{x} = (x, y)^T$ . As base scheme we use the method from [25].

The evolution equation for the magnetic potential reduces to the system

$$\begin{aligned}\mathbb{A}_{,t}^1 - u^2 \mathbb{A}_{,x}^2 - u^3 \mathbb{A}_{,x}^3 + u^2 \mathbb{A}_{,y}^1 &= 0, \\ \mathbb{A}_{,t}^2 + u^1 \mathbb{A}_{,x}^2 - u^1 \mathbb{A}_{,y}^1 - u^3 \mathbb{A}_{,y}^3 &= 0, \\ \mathbb{A}_{,t}^3 + u^1 \mathbb{A}_{,x}^3 + u^2 \mathbb{A}_{,y}^3 &= 0.\end{aligned}\tag{56}$$

The magnetic field can be obtained via  $\mathbf{B} = (\mathbb{A}_{,y}^3, -\mathbb{A}_{,x}^3, \mathbb{A}_{,x}^2 - \mathbb{A}_{,y}^1)^T$ . Since  $B_{,z}^3 = 0$ , we can obtain a divergence free magnetic field by implying a constrained transport algorithm which only updates  $B^1$  and  $B^2$  and which uses  $B^3$  from the base scheme. Since the first two components of the magnetic field only depend on  $\mathbb{A}^3$ , we just need to solve a scalar hyperbolic evolution equation for  $\mathbb{A}^3$ , i.e.

$$\mathbb{A}_{,t}^3 + u^1 \mathbb{A}_{,x}^3 + u^2 \mathbb{A}_{,y}^3 = 0.\tag{57}$$

On the other hand we can test the three-dimensional method by approximating the system (56) using the dimensional split approach outlined in §5.2 and updating  $B^1$ ,  $B^2$  and  $B^3$  in each time step. Numerical results for the 2.5 dimensional case will be discussed in §6.1.1 and §6.1.2.

## 6. Numerical experiments

We present several numerical experiments in this section. All the numerical tests are carried out in the CLAWPACK software package [19], which can be freely downloaded from the following website:

<http://www.clawpack.org>.

In particular, the current work has been incorporated into the MHDCLAW extension of CLAWPACK, which was originally developed by Rossmanith. This extension can also be freely downloaded from the web:

<http://www.math.wisc.edu/~rossmani/MHDCLAW/>.

### 6.1. Test cases in 2.5D

We begin by presenting numerical results for two problems in 2.5 dimensions (i.e., the solution depends on only on the independent variables  $(x, y, t)$ , but all three components of the velocity and magnetic field vectors are non-zeros). The two examples that are considered are:

1. Smooth Alfvén wave;
2. Cloud-shock interaction.

The first example involves an infinitely smooth exact solution of the ideal MHD system. The second example involves the interaction of a high-pressure shock interacting with a high-density bubble (i.e., a discontinuous example).

Mesh	$L_\infty$ Error in $B^1$	$L_\infty$ Error in $B^2$	$L_\infty$ Error in $B^3$
$64 \times 128$	$6.731 \times 10^{-4}$	$2.38 \times 10^{-3}$	$1.296 \times 10^{-2}$
$128 \times 256$	$1.684 \times 10^{-4}$	$5.952 \times 10^{-4}$	$3.237 \times 10^{-3}$
$256 \times 512$	$4.231 \times 10^{-5}$	$1.493 \times 10^{-4}$	$8.085 \times 10^{-4}$
<b>Order</b>	1.996	1.998	2.001

Mesh	$L_\infty$ Error in $A^1$	$L_\infty$ Error in $A^2$	$L_\infty$ Error in $A^3$
$64 \times 128$	$1.294 \times 10^{-2}$	$1.287 \times 10^{-2}$	$1.421 \times 10^{-2}$
$128 \times 256$	$3.228 \times 10^{-3}$	$3.222 \times 10^{-3}$	$3.552 \times 10^{-3}$
$256 \times 512$	$8.063 \times 10^{-4}$	$8.060 \times 10^{-4}$	$8.878 \times 10^{-4}$
<b>Order</b>	2.003	1.997	2.000

Table 1: Error tables for the 2.5-dimensional Alfvén problem at time  $t = 1.5$  using proposed dimensional split scheme. This table shows that all components of the magnetic field and all components of the magnetic potential converge at second order accuracy.

### 6.1.1. Smooth Alfvén wave problem

We first verify the order of convergence of the constrained transport method for a smooth circular polarized Alfvén wave which propagates in direction  $\mathbf{n} = (\cos \phi, \sin \phi, 0)^T$  towards the origin. This problem has been considered by several authors (e.g., [25, 30]), and is a special case ( $\theta = 0$ ) of the 3D problem described in detail §6.2.1. Suffice it to say in this section that the solution consists of a sinusoidal wave propagating at constant speed without changing shape, thus making it a prime candidate to verify order of accuracy.

In Table 1, we show the convergence rates for the 2.5 dimensional test problem. Here all three components of the magnetic field have been updated in the constrained transport method and the magnetic potential was approximated using a dimensional split method for (56). The table clearly shows that the proposed method is second-order accurate in all of the magnetic field, as well as the magnetic potential components.

### 6.1.2. Cloud-shock interaction problem

Next we consider a problem with a strong shock interacting with a relatively large density jump in the form of a high-density bubble that is at rest with its background before the shock-interaction. This problem has also been considered by several authors (e.g., [25, 30]), however, in previous work a solution was always obtained by treating  $B^3$  as a standard conserved variable. Here we compare such an approach, in the form of the method described in [25], against the method that is proposed in the current work. In our new method all three components of the magnetic field are computed from derivatives of the magnetic vector potential. The details of the initial conditions are written in §6.2.3.

In Figure 1 we show numerical results for the 2.5 dimensional problem. We compare the scheme from [25] which only updates  $B^1$  and  $B^2$  using the scalar evolution equation for the vector potential (57) with the new constrained

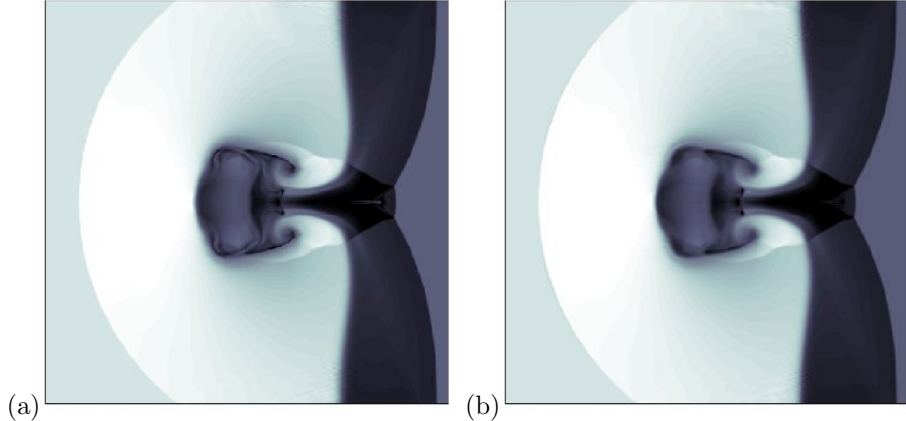


Figure 1: The 2.5-dimensional cloud-shock interaction problem. Shown here are the out-of-plane magnetic field at time  $t = 0.06$  as calculated on a  $512 \times 512$  mesh using (a) the scheme of [25] that only uses  $\mathbb{A}^3$ , and (b) the proposed scheme using the full vector potential  $\mathbb{A}$ .

transport method which updates all components of the magnetic field. Although these methods compute  $B^3$  in very different ways, using very different limiters, these plots show that they nonetheless produce similar solutions. This result gives us confidence that the proposed method is able to accurately resolve strong shocks despite the somewhat unusual approach for approximating the magnetic field.

### 6.2. Test cases in 3D

We present numerical results for three-dimensional versions of three classical MHD test problems:

1. Smooth Alfvén wave;
2. Orszag-Tang vortex;
3. Cloud-shock interaction.

Two-dimensional versions of these problems have been studied by many authors, see for instance [25, 30].

Our test calculations will all be based on the splitting (44). We also carried out several tests with (43); however, we will not report those here. The two methods produced comparable results.

#### 6.2.1. Smooth Alfvén wave problem

We first verify the order of convergence of the constrained transport method for a smooth circular polarized Alfvén wave which propagates in direction  $\mathbf{n} = (\cos \phi \cos \theta, \sin \phi \cos \theta, \sin \theta)^T$  towards the origin. Here  $\phi$  is an angle with respect to the  $x$ -axis in the  $x$ - $y$ -plane and  $\theta$  is an angle with respect to the  $x$ - $z$ -plane. Initial values for the velocity and the magnetic field are specified in

the direction  $\mathbf{n}$  as well as the orthonormal directions  $\mathbf{t} = (-\sin \phi, \cos \phi, 0)^T$  and  $\mathbf{r} = (-\cos \phi \sin \theta, -\sin \phi \sin \theta, \cos \theta)^T$ :

$$\begin{aligned} u_n(0, \mathbf{x}) &= 0, \quad B_n(0, \mathbf{x}) = 1, \\ u_t(0, \mathbf{x}) &= B_t(0, \mathbf{x}) = 0.1 \sin(2\pi \mathbf{n} \cdot \mathbf{x}), \\ u_r(0, \mathbf{x}) &= B_r(0, \mathbf{x}) = 0.1 \cos(2\pi \mathbf{n} \cdot \mathbf{x}). \end{aligned}$$

Density and pressure are constant and set to  $\rho(0, \mathbf{x}) = 1$ ,  $p(0, \mathbf{x}) = 0.1$ . The Alfvén wave speed is  $|v_A| = B_n/\sqrt{\rho} = 1$ , i.e. the flow agrees with the initial state whenever the time is an integer value. In Cartesian coordinates velocity and magnetic field are given by

$$\begin{aligned} \mathbf{u}(0, \mathbf{x}) &= u_n \mathbf{n} + u_t \mathbf{t} + u_r \mathbf{r}, \\ \mathbf{B}(0, \mathbf{x}) &= B_n \mathbf{n} + B_t \mathbf{t} + B_r \mathbf{r}. \end{aligned}$$

Our initial values for the magnetic potential are

$$\begin{aligned} \mathbb{A}^1(0, \mathbf{x}) &= z \sin \phi \cos \theta - \frac{1}{20\pi} \sin \phi \sin(2\pi \mathbf{n} \cdot \mathbf{x}), \\ \mathbb{A}^2(0, \mathbf{x}) &= x \sin \theta + \frac{1}{20\pi} \cos \phi \sin(2\pi \mathbf{n} \cdot \mathbf{x}), \\ \mathbb{A}^3(0, \mathbf{x}) &= y \cos \phi \cos \theta + \frac{1}{20\pi \cos \theta} \cos(2\pi \mathbf{n} \cdot \mathbf{x}). \end{aligned}$$

The computational domain is chosen such that it contains one period of the wave, i.e. we compute in the domain

$$\left[0, \frac{1}{\cos \phi \cos \theta}\right] \times \left[0, \frac{1}{\sin \phi \cos \theta}\right] \times \left[0, \frac{1}{\sin \theta}\right],$$

and impose periodicity in all directions. Here we use  $\theta = \phi = \tan^{-1}(0.5) \approx 26.5651^\circ$ . By setting  $\theta = 0$ , we obtain the initial data for the 2.5 dimensional case. Note that while the conserved quantities  $(\rho, \rho \mathbf{u}, \mathcal{E}, \mathbf{B})$  are periodic, the magnetic potential consists of a linear part and a periodic part. For periodic boundary conditions, the linear part is linearly extrapolated to ghost cells, while the periodic part is handled by a periodic extension of the appropriate grid cell values to the ghost cells.

In Table 2 we show the results of a numerical convergence study in the three-dimensional case which confirm that our method is of second order.

### 6.2.2. Orszag-Tang vortex

Our next test problem is the Orszag-Tang vortex problem. This is a standard test case for the two-dimensional MHD equations. Here we add a small perturbation to the initial velocity field which depends on the vertical direction.

The initial data have the form  $\rho(0, \mathbf{x}) = \gamma^2$ ,  $p(0, \mathbf{x}) = \gamma$ ,

$$\begin{aligned} \mathbf{u}(0, \mathbf{x}) &= (-\sin y(1 + \varepsilon \sin z), \sin x(1 + \varepsilon \sin z), \varepsilon \sin(z))^T, \\ \mathbf{B}(0, \mathbf{x}) &= (-\sin y, \sin(2x), 0)^T. \end{aligned}$$

Mesh	$L_\infty$ Error in $\mathbf{B}^1$	$L_\infty$ Error in $\mathbf{B}^2$	$L_\infty$ Error in $\mathbf{B}^3$
$16 \times 32 \times 32$	$1.022 \times 10^{-2}$	$2.787 \times 10^{-2}$	$2.382 \times 10^{-2}$
$32 \times 64 \times 64$	$2.577 \times 10^{-3}$	$7.075 \times 10^{-3}$	$6.101 \times 10^{-3}$
$64 \times 128 \times 128$	$6.487 \times 10^{-4}$	$1.782 \times 10^{-3}$	$1.549 \times 10^{-3}$
<b>Order</b>	1.990	1.989	1.979

Mesh	$L_\infty$ Error in $\mathbb{A}^1$	$L_\infty$ Error in $\mathbb{A}^2$	$L_\infty$ Error in $\mathbb{A}^3$
$16 \times 32 \times 32$	$1.902 \times 10^{-1}$	$1.460 \times 10^{-1}$	$1.187 \times 10^{-1}$
$32 \times 64 \times 64$	$4.816 \times 10^{-2}$	$3.747 \times 10^{-2}$	$2.995 \times 10^{-2}$
$64 \times 128 \times 128$	$1.220 \times 10^{-2}$	$9.528 \times 10^{-3}$	$7.564 \times 10^{-3}$
<b>Order</b>	1.980	1.975	1.985

Table 2: Error tables for the 3-dimensional Alfvén problem at time  $t = 1$ . This table shows that all components of the magnetic field and all components of the magnetic potential converge at second order accuracy. For the computation of the order we used the errors computed on the second and third grid.

Here we used  $\varepsilon = 0.2$ . The initial values for the magnetic potential are

$$\mathbb{A}(0, \mathbf{x}) = (0, 0, \cos y + \cos(2x))^T.$$

The computational domain is a cube with side length  $2\pi$ . Periodicity is imposed in all three directions.

In Figures 2-5 we show a sequence of schlieren plots of the pressure for several slices of data in the  $x$ - $y$ -plane for  $z = \pi/2, \pi, 3\pi/2$ . Those computations have been performed with the high-resolution constrained transport method with monotonized central limiter and the diffusive limiter using  $\nu = 0.3$ . In Figures 6, 7 we show schlieren plots of pressure in the  $x$ - $y$ -plane for  $z = \pi$  at different times.

### 6.2.3. Cloud-shock interaction problem

Finally we consider the cloud-shock interaction problem. The initial conditions consist of a shock which is located at  $x = 0.05$ ,

$$\begin{aligned} & (\rho, u^1, u^2, u^3, p, B^1, B^2, B^3)(0, \mathbf{x}) \\ &= \begin{cases} (3.86859, 11.2536, 0, 0, 167.345, 0, 2.1826182, -2.1826182) & : x < 0.05 \\ (1, 0, 0, 0, 1, 0, 0.56418958, 0.56418958) & : x \geq 0.05. \end{cases} \end{aligned}$$

A spherical cloud of density  $\rho = 10$  and radius  $r = 0.15$  is initially centered at  $(0.25, 0.5, 0.5)$ . The cloud is in hydrostatic equilibrium with the fluid to the right of the shock. The magnetic potential has initially the form

$$\mathbb{A}(0, \mathbf{x}) = \begin{cases} (2.1826182y, 0, -2.1826182(x - 0.05))^T & : x < 0.05 \\ (-0.56418958y, 0, 0.56418956(x - 0.05))^T & : x \geq 0.05. \end{cases}$$

This test problem can be computed in the unit cube with inflow boundary conditions on the left side and outflow conditions on all other sides. Instead we

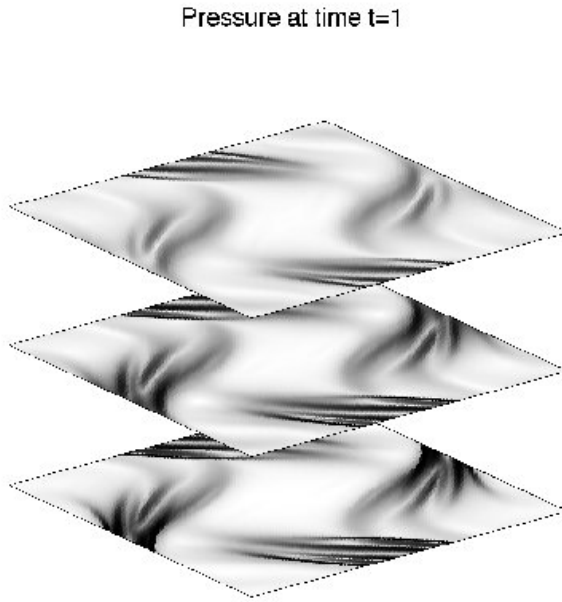


Figure 2: Schlieren plots of pressure for the 3D Orzsag-Tang problem at time  $t = 1$  computed on a grid with  $150 \times 150 \times 150$  grid points. Slices of the solution at  $z = \pi/2, \pi, 3\pi/2$  in the  $x$ - $y$ -plane are shown.

make use of the symmetry of the problem and compute the problem only in a quarter of the full domain, i.e. in  $[0, 1] \times [0.5, 1] \times [0.5, 1]$  and impose reflecting boundary conditions at the lower boundary in the  $y$  and the  $z$  direction. For the conserved quantities, the reflecting boundary condition is implemented in the standard way, i.e. by copying the values of the conserved quantities from the first grid cells of the flow domain to the ghost cells. The normal momentum component in the ghost cells is negated. The components of the magnetic potential are linearly extrapolated to the ghost cells.

In the 2.5 dimensional case a circular cloud of density  $\rho = 10$  and radius  $r = 0.15$  is initially centered at  $(0.25, 0.5)$ . In this case the computational domain is the unit square.

In Figures 8 and 9, we show a sequence of schlieren plots of the density in the  $x$ - $y$ -plane for  $z = 0.5$  and the  $x$ - $z$ -plane for  $y = 0.5$ . The three-dimensional radial symmetric solution structure compares well with previously shown two-dimensional computations. In Figures 10 and 11 we show the schlieren plots of density in the  $x$ - $z$ -plane. Here the diffusive limiter described in §5.2 was used with  $\nu = 0.02$ .

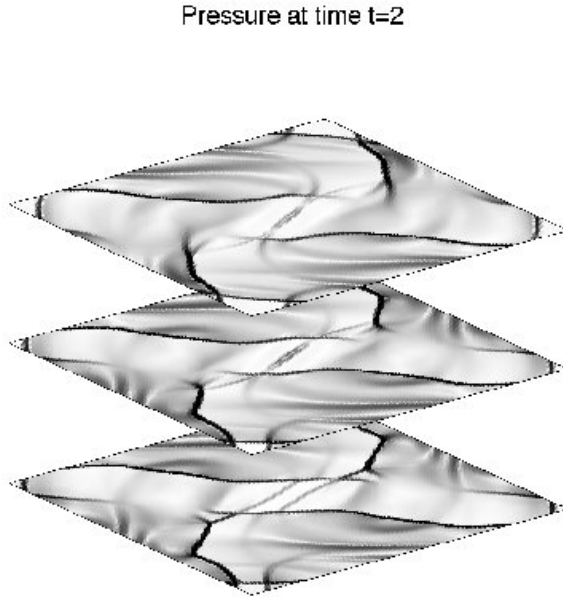


Figure 3: Schlieren plots of pressure for the 3D Orzsag-Tang problem at time  $t = 2$  computed on a grid with  $150 \times 150 \times 150$  grid points. Slices of the solution at  $z = \pi/2, \pi, 3\pi/2$  in the  $x$ - $y$ -plane are shown.

## 7. Conclusions

We have presented a new constrained transport method for the three-dimensional MHD equations. Depending on the gauge condition, we discussed different possible evolution equations for the magnetic potential. All of these gauge conditions implicate some difficulties for the discretization. The condition used here leads to a weakly hyperbolic system for the evolution of the magnetic potential. We discretized this system with a splitting approach. For the MHD equations we used a wave propagation method. Several numerical tests confirm the robustness and accuracy of the resulting constrained transport scheme.

Our method is fully explicit, as well as fully unstaggered, and therefore well-suited for adaptive mesh refinement and parallelization.

**Acknowledgements.** The authors would like to thank Prof. Dr. Rainer Grauer from the Ruhr-Universität-Bochum for several useful discussions. This work was supported in part by NSF grants DMS-0711885 and DMS-1016202 and by the DFG through FOR1048.

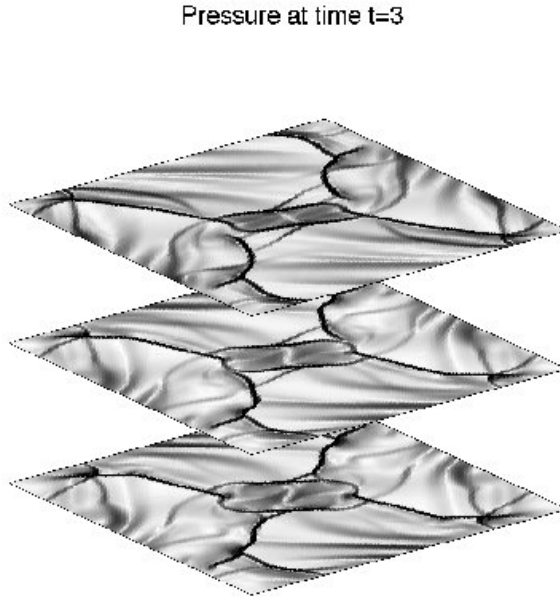


Figure 4: Schlieren plots of pressure for the 3D Orzsag-Tang problem at time  $t = 3$  computed on a grid with  $150 \times 150 \times 150$  grid points. Slices of the solution at  $z = \pi/2, \pi, 3\pi/2$  in the  $x$ - $y$ -plane are shown.

## References

- [1] D.S. Bale, R.J. LeVeque, S. Mitran, and J.A. Rossmanith. A wave propagation method for conservation laws and balance laws with spatially varying flux functions. *SIAM J. Sci. Comp.*, 24:955–978, 2003.
- [2] D.S. Balsara. Second-order-accurate schemes for magnetohydrodynamics with divergence-free reconstruction. *Astrophys. J. Suppl.*, 151:149–184, 2004.
- [3] D.S. Balsara and J. Kim. A comparison between divergence-cleaning and staggered-mesh formulations for numerical magnetohydrodynamics. *Astrophys. J.*, 602:1079—1090, 2004.
- [4] D.S. Balsara and D. Spicer. A staggered mesh algorithm using high order Godunov fluxes to ensure solenoidal magnetic fields in magnetohydrodynamic simulations. *J. Comp. Phys.*, 149(2):270–292, 1999.
- [5] T.J. Barth. On the role of involutions in the discontinuous Galerkin discretization of Maxwell and magnetohydrodynamic systems. In *IMA Volume on Compatible Spatial Discretizations*, volume 142. Springer-Verlag, 2005.

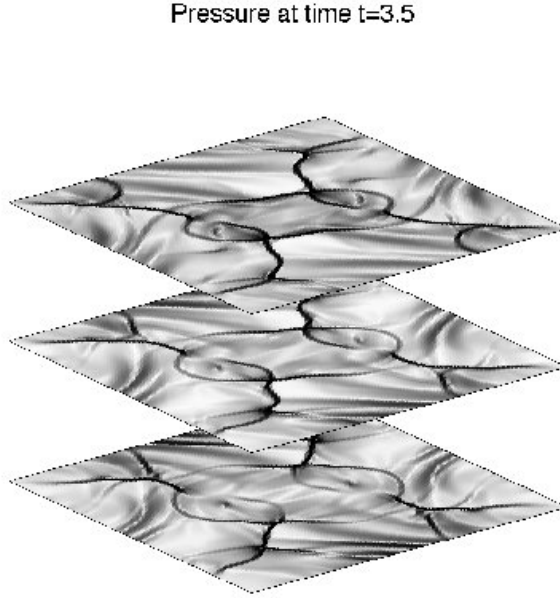


Figure 5: Schlieren plots of pressure for the 3D Orszag-Tang problem at time  $t = 3.5$  computed on a grid with  $150 \times 150 \times 150$  grid points. Slices of the solution at  $z = \pi/2, \pi, 3\pi/2$  in the  $x$ - $y$ -plane are shown.

- [6] J.U. Brackbill and D.C. Barnes. The effect of nonzero  $\nabla \cdot \mathbf{B}$  on the numerical solution of the magnetohydrodynamic equations. *J. Comp. Phys.*, 35:426–430, 1980.
- [7] P. Cargo and G. Callice. Roe matrices for ideal MHD and systematic construction of Roe matrices for systems of conservation laws. *J. Comp. Phys.*, 136:446–466, 1997.
- [8] F.F. Chen. *Introduction to Plasma Physics and Controlled Fusion*. Plenum Press, 1984.
- [9] C. Dafermos. *Hyperbolic Conservation Laws in Continuum Physics*. Springer, 2010.
- [10] W. Dai and P.R. Woodward. A simple finite difference scheme for multidimensional magnetohydrodynamic equations. *J. Comp. Phys.*, 142(2):331–369, 1998.
- [11] A. Dedner, F. Kemm, D. Kröner, C.-D. Munz, T. Schnitzer, and M. Wessenberg. Hyperbolic divergence cleaning for the MHD equations. *J. Comp. Phys.*, 175:645–673, 2002.

- [12] C. Evans and J.F. Hawley. Simulation of magnetohydrodynamic flow: A constrained transport method. *Astrophys. J.*, 332:659–677, 1988.
- [13] M. Fey and M. Torrilhon. A constrained transport upwind scheme for divergence-free advection. In T.Y. Hou and E. Tadmor, editors, *Hyperbolic Problems: Theory, Numerics, and Applications*, pages 529–538. Springer, 2003.
- [14] S.K. Godunov. Symmetric form of the magnetohydrodynamic equations. *Numerical Methods for Mechanics of Continuum Medium*, 1:26–34, 1972.
- [15] T.I. Gombosi. *Physics of the Space Environment*. Cambridge University Press, 1998.
- [16] J.O. Langseth and R.J. LeVeque. A wave propagation method for three-dimensional hyperbolic conservation laws. *J. Comp. Phys.*, 165:126–166, 2000.
- [17] R.J. LeVeque. *Finite Volume Methods for Hyperbolic Problems*. Cambridge University Press, 2002.
- [18] R.J. LeVeque. Wave propagation algorithms for multi-dimensional hyperbolic systems. *J. Comp. Phys.*, 131:327–335, 1997.
- [19] R.J. LeVeque. CLAWPACK software, available from <http://www.amath.washington.edu/~claw>
- [20] P. Londrillo and L. Del Zanna. On the divergence-free condition in godunov-type schemes for ideal magnetohydrodynamics: the upwind constrained transport method. *J. Comp. Phys.*, 195:17–48, 2004.
- [21] G.K. Parks. *Physics of Space Plasmas: An Introduction*. Addison-Wesley, 1991.
- [22] P.-O. Persson and J. Peraire. Sub-cell shock capturing for discontinuous Galerkin methods. *AIAA*, 2006.
- [23] K.G. Powell. An approximate Riemann solver for magnetohydrodynamics (that works in more than one dimension). Technical Report 94-24, ICASE, Langley, VA, 1994.
- [24] K.G. Powell, P.L. Roe, T.J. Linde, T.I. Gombosi, and D.L. De Zeeuw. A solution-adaptive upwind scheme for ideal magnetohydrodynamics. *J. Comp. Phys.*, 154:284–309, 1999.
- [25] J.A. Rossmanith. An unstaggered, high-resolution constrained transport method for magnetohydrodynamic flows. *SIAM J. Sci. Comp.*, 28:1766–1797, 2006.

- [26] D.S. Ryu, F. Miniati, T.W. Jones, and A. Frank. A divergence-free upwind code for multidimensional magnetohydrodynamic flows. *Astrophys. J.*, 509(1):244–255, 1998.
- [27] H. De Sterck. Multi-dimensional upwind constrained transport on unstructured grids for “shallow water” magnetohydrodynamics. In *Proceedings of the 15th AIAA Computational Fluid Dynamics Conference, Anaheim, California*, page 2623. AIAA, 2001.
- [28] P.K. Sweby. High resolution schemes using flux limiters for hyperbolic conservation laws. *SIAM J. Num. Anal.*, 21: 995-1011, 1984.
- [29] E. Tadmor. Entropy stability theory for difference approximations of nonlinear conservation laws and related time-dependent problems. *Acta Numerica*, 12:451–512, 2003.
- [30] G. Tóth. The  $\nabla \cdot B = 0$  constraint in shock-capturing magnetohydrodynamics codes. *J. Comp. Phys.*, 161:605–652, 2000.
- [31] K. Yee. Numerical solutions of initial boundary value problems involving Maxwell’s equations in isotropic media. *IEEE Transactions on Antennas and Propagation*, AP-14:302–307, 1966.

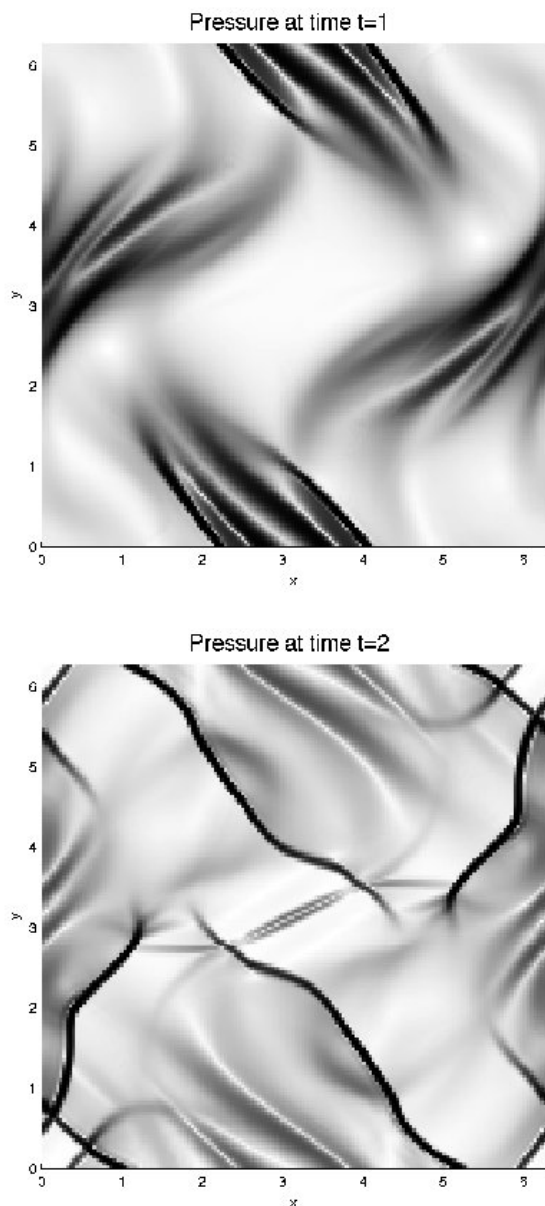


Figure 6: Schlieren plots of pressure for the 3D Orzsag-Tang vortex problem at time  $t = 1$  and  $= 2$  computed on a grid with  $150 \times 150 \times 150$  grid points. Slices of the solution at  $z = \pi$  in the  $x$ - $y$ -plane are shown.

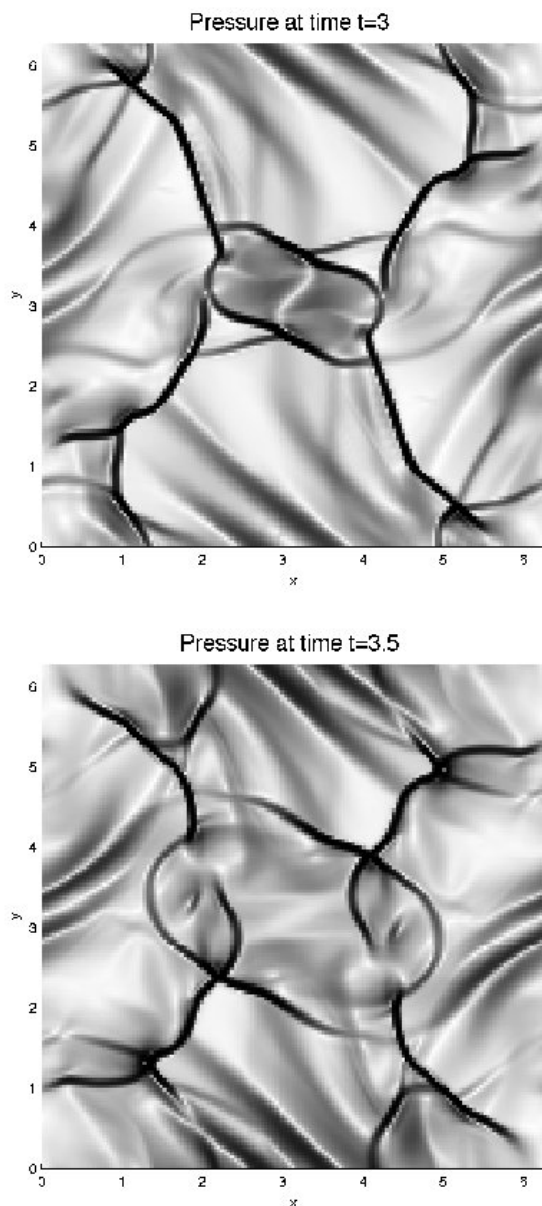


Figure 7: Schlieren plots of pressure for the 3D Orzsag-Tang vortex problem at time  $t = 3$  and  $t = 3.5$  computed on a grid with  $150 \times 150 \times 150$  grid points. Slices of the solution at  $z = \pi$  in the  $x$ - $y$ -plane are shown.

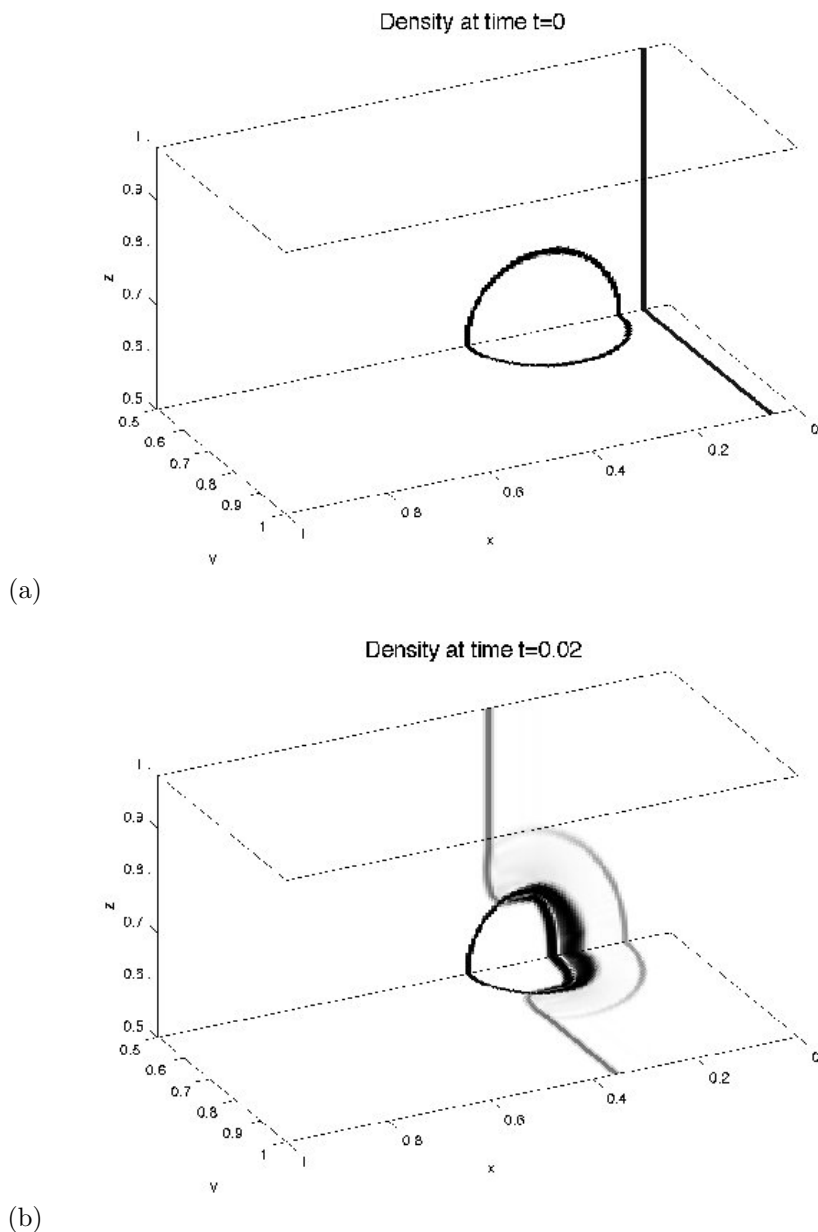


Figure 8: Sequence of schlieren plots of density for the 3-dimensional cloud-shock interaction problem using a mesh with  $200 \times 100 \times 100$  grid cells. Shown here is the solution in two selected orthogonal planes.

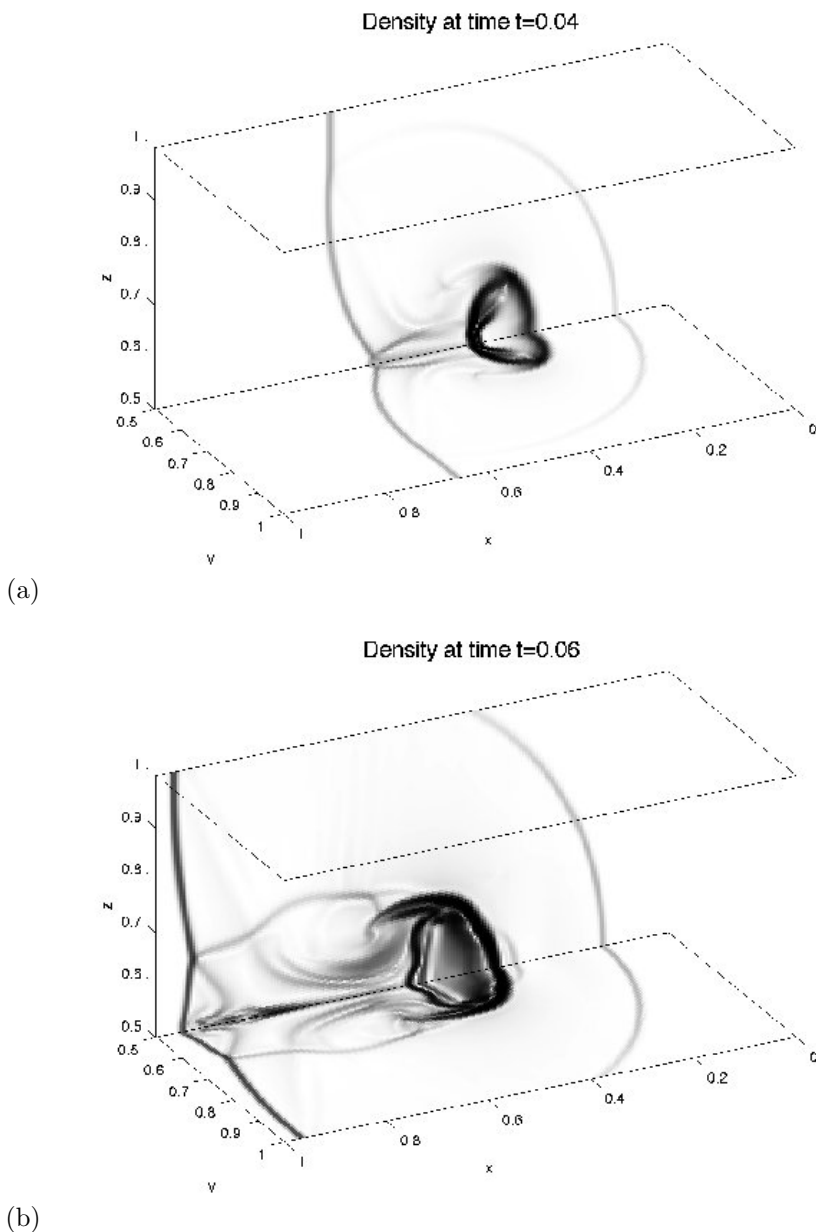


Figure 9: Sequence of schlieren plots of density for the 3-dimensional cloud-shock interaction problem using a mesh with  $200 \times 100 \times 100$  grid cells. Shown here is the solution in two selected orthogonal planes.

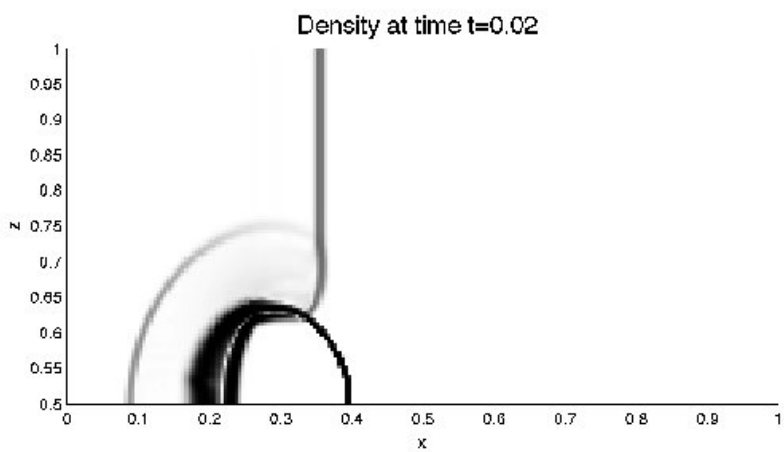
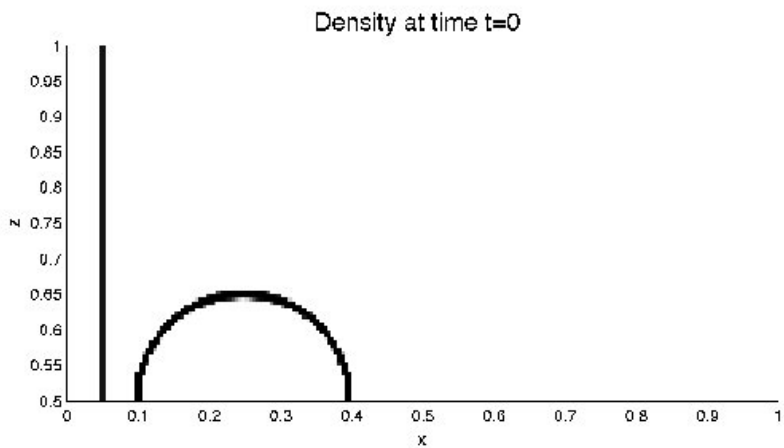


Figure 10: Sequence of schlieren plots of density in the  $x$ - $z$ -plane for  $y = 0.5$  at time 0 and 0.02.

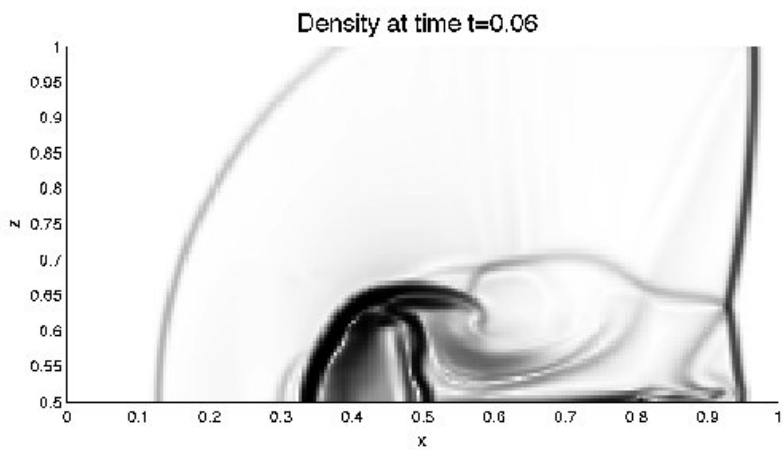
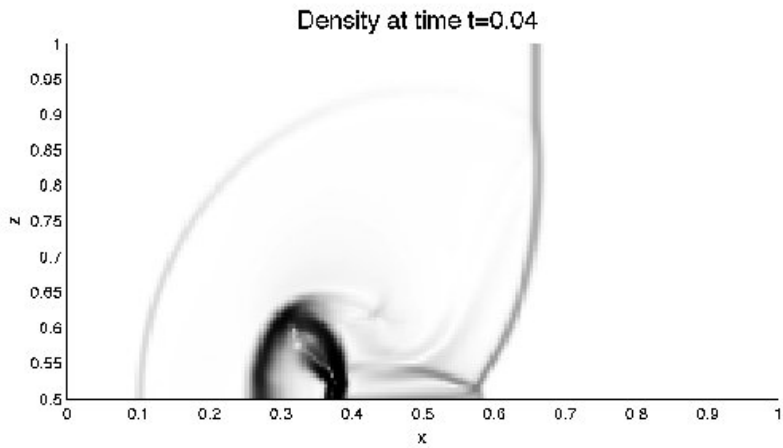


Figure 11: Sequence of schlieren plots of density in the  $x$ - $z$ -plane for  $y = 0.5$  at time 0.04 and 0.6.